The inelastic scattering of electrons by protons*

by

A. Cone,** K. W. Chen,† J.R. Dunning,‡ N. F. Ramsey, J. K. Walker and Richard Wilson

Harvard University, Cambridge, Massachusetts

ABSTRACT

The inelastic scattering of electrons by protons has been measured at incident electron energies up to 5 BeV/c and momentum transfers $q^2=4(\text{BeV/c})^2$. Excitation of known nucleon resonances at M=1238, 1512, 1688 and possibly 1920 MeV have been observed.

The calculations for the resonance at M=1238 MeV have been compared with calculations by Adler based on the dispersion theory of Chew, Goldberger, Low and Nambu. The agreement is good. Qualitative models are discussed for the other resonances.

*Supported by the United States Atomic Energy Commission

†Presently at Palmer Physical Laboratory, Princeton University, Princeton, New Jersey.

**Presently at Vancouver City College, Vancouver, British Columbia.

‡Supported by the National Science Foundation at the time of this experiment

DISCLAIMER

INTRODUCTION

The inelastic scattering of electrons was shown to be a useful technique for studying atomic structure by Franck and Hertz. By studying the energy spectrum of scattered electrons they were able to measure the excitation spectrum of atoms. In the terminology of modern high energy physics, this would now be called missing mass spectroscopy.

The application of this method to the study of the proton and its excited states was begun by Panofsky and Allton[1] and was extended by Hand[2]. These authors studied the excitation of the pion-nucleon (nucleon excited state) at a mass of 1240 MeV and with quantum numbers, $I=3/2$, $J=3/2^+$ up to a momentum transfer $q^2=18\ f^{-2}$ $\left(0.7(\text{BeV/c})^2\right)$. Hand failed to find evidence of excitation of other resonances.

In this work, the excitation of the 1240 MeV resonance is studied up to a momentum transfer $q^2=90$ fermi^{-2} $\left(3.61(\text{BeV/c})^2\right)$ and the excitation of the resonances at masses of 1512 MeV, 1690 MeV and 1920 MeV are observed. These are compared with such theoretical calculations as are available. There is good agreement except for the excitation of the resonance at 1512 MeV which is too great to be understood.

KINEMATICS AND ONE PHOTON EXCHANGE

Throughout this paper we will use a notation close to that of Hand[2]. Some of the kinematic quantities are clear from the diagram of Fig. 1. At these momentum transfers, elastic scattering is believed to proceed primarily by one photon exchange. It is therefore reasonable to assume that the inelastic scattering also proceeds by one photon exchange. Then the cross section for inelastic scattering can be shown to be separable[2].

$$\frac{d^2\sigma}{d\Omega dE_f} = \Gamma_{transverse}(\theta, q^2, K)\, \sigma_{transverse}(q^2, K) + \Gamma_{scalar}(\theta, q^2, K)\, \sigma_{scalar}(q^2, K) \qquad (1)$$

where

$$\Gamma_{transverse} = \Gamma_T = \frac{\alpha}{4\pi^2}\,\frac{K}{q^2}\,\frac{E_f}{E_i}\left[2 + \frac{\cot^2(\theta/2)}{1 + (q_o^2/q^2)}\right]$$

$$\Gamma_{scalar} = \Gamma_o = \frac{\alpha}{4\pi^2}\,\frac{K}{q^2}\,\frac{E_f}{E_i}\,\frac{2\cot^2(\theta/2)}{1 + (q_o^2/q^2)}$$

$$K = q_o - q^2/2M = \frac{M^{*2} - M^2}{2M}$$

The relation between K and M^* is independent of the 4-momentum transfer q^2. At $q^2=0$ (photoproduction), K is the laboratory photon energy. For electroproduction it is therefore called the virtual photon energy.

In the metric used here, the square of the 4-momentum transfer is positive for scattering:

$$q^2 = 4E_i E_f \sin^2(\theta/2) \qquad 2$$

If we use quantities in the centre of mass of the outgoing nucleon system M^* we find the fourth component of the 4-vector q

$$q_o^* = \frac{M^{*2} - M^2}{2M^*} - q^2/2M^* \qquad 3$$

whereas, in the laboratory:

$$q_o = \frac{M^{*2} - M^2}{2M} + q^2/2M \qquad 4$$

The normalization of the Γ factors is such that:

$$\sigma_T(0, K) = \sigma_\gamma(K) \qquad 5$$

which is the photoproduction cross section at the photon energy K. The Γ factors have the dimensions of the number of virtual photons

per BeV steradian.

The experimental aim is therefore to determine $\sigma_T(q^2, K)$ and $\sigma_o(q^2, K)$ over a range of values of q^2 and K. (Or, equivalently, q^2 and M^*.)

APPARATUS

The experiment was done concurrently with the experiments on elastic electron proton and quasielastic electron deuteron scattering previously reported[3,4] and used the same apparatus.

The electrons from the internal beam of the Cambridge Electron Accelerator impinged on a liquid hydrogen target; the scattered electrons passed through a quadrupole spectrometer onto a scintillation counter bank. A threshold Cerenkov counter and a shower counter helped to distinguish electrons from pions. Pions could be detected by knock on (π-e scattering) in the Cerenkov counter and by charge exchange in the shower counter.

Figs. 2 and 3 are vertical and horizontal schemes of the experimental setup. The liquid hydrogen target was contained in a vertical cylinder of Mylar or Dupont H-film which was centered about 3/4" inside the equilibrium orbit of the circulating beam. At the

end of the acceleration cycle the r.f. was turned off and the electrons spiraled inward until they penetrated the target. The incident flux was monitored by a quantameter and an ion chamber which observed the forward Bremsstrahlung from the electron beam hitting the target.

The scattered electrons passed through a single quadrupole magnet with a center plug and were focussed along a horizontal line. Several long thin scintillator counters were arranged parallel to this line thus making available several momentum acceptance bins simultaneously. After these "slat" counters, as they were called, was a gas Cerenkov counter which was used as a threshhold counter to distinguish electrons from heavier charged particles. Finally, there were two large scintillator counters, the latter of which was used as a shower counter to distinguish the high energy scattered electrons from low energy knock-on electrons and pions.

An electron was counted when the following conditions were met. Counters C_1, C_8, and either C_{sa}, C_{7a} or C_{sb}, C_{7B} had to register in coincidence which meant a charged particle had crossed the median plane of the quadrupole magnet somewhere between C_s and C_7. Such an event was called a fourfold count. A count from C_9 was demanded in coincidence with this; such an event was called a fivefold. A

count from the Cerenkov counter in coincidence with a fivefold, opened a gate to the pulse height analyzer to receive the output from the shower counter C_{10}. If the signal from the shower counter was above the bias level set for it, then the coincidence of fivefold plus Cerenkov plus C_{10}, called a slat drive signal, was produced. If a slat counter, i.e., counters C_2 thru C_6, registered in coincidence with the slat drive signal, an electron count was registered in the appropriate momentum bin.

This apparatus has been described in great detail in Ref. (3) and (4). Some additional details of importance for the inelastic spectrum follow.

Spectrometer Calibration

The magnetic field gradient and effective length of the quadrupole magnet as a function of current were supplied to an accuracy of 0.2% by Paul Cooper, Jr. These we measured by a long flip coil and by Hall probe measurements. A graphical interpolation of these points was the basis for calculating the curve of of scattered energy focussed at a distance of 63" from the face of the magnet (the center of C_4 in Fig. 3) vs. the current through the magnet. This curve was recalibrated by noting the position of the

elastic peak as a function of the spectrometer current. The recalibrated curve shows that the magnet did not saturate as rapidly as the interpolation of Cooper's data would suggest.

At the focal point of 63", the average percentage change in momentum is .718% per inch.

Now the slat counters (C_2 thru C_6 in Fig 3) were 1.5" wide in the direction of momentum resolution and this corresponds to about 1.1% for dp/p. However, because of their finite height (1/16") the slats detected particles outside this momentum bite. So, in order to compute the momentum resolution properly, the efficiency of the slat counters must be taken into account. The method is as follows. Take a portion of the spectrum which is relatively flat. Let N equal the number of bins in which counts are accepted. Suppose there are really n counts per bin. Then Nn is the ideal total number of counts. Let f be the fractional overlap on one side of a slat into the next bin. Let S equal the sum of the actual slat counts; let T equal the total in peak, i.e. the number of events which triggered any or all of the slats simultaneously.

Then we have $Nn(1+2f) = sS$

and $Nn + n2f = T$ 6

hence $2f = N(S - T)/(NT - S)$.

Then 1.08% times $(1 + 2f)$ is the actual dp/p for the slats.

This method implies no more than about a 5% error in the momentum bite per slat.

The counter bank tilt

The small but finite angular acceptance of the spectrometer led to a spread in the energy of scattered electrons. During the experiment the slats were ~~inclined from the perpendicular to the spectrometer axis~~ tilted in the horizontal plane so that all the elastic events would appear in one slat (neglecting resolution function and radiative tails for the present). The same tilt of the counter bank also insured that all inelastically scattered electrons of the same value of K appeared in the same slat. We see this from a kinematic calculation as follows.

$$E' = \frac{E - K}{1 + \frac{E}{M}(1 - \cos\theta)} \; ; \quad \frac{\partial E'}{\partial \theta} = - E' \frac{\frac{E}{M}\sin\theta}{1 + \frac{E}{M}(1 - \cos\theta)}$$

7

$$\therefore \frac{dE'}{E'} = - \frac{\frac{E}{M}\sin\theta}{1 + \frac{E}{M}(1 - \cos\theta)} d\theta$$

which is independent of E' and K for constant E.

Fig. 4 shows the calculated resolution of the spectrometer compared with the measured elastic scattering.

Pion Rejection

High energy pions have a mean free path of about eight inches in lead and could, therefore, be counted in the spectrometer not only by traversing the spectrometer according to the design, but also by penetrating the shielding and the central plug. The background of these pions was very large.

Pions could count in the threshold Cerenkov counter by their knock on electrons - particularly if they had penetrated the absorber. They could count in the shower counter by cahrge exchange. It was important to ensure that pions were not being detected in this experiment.

In the elastic scattering experiment[3] absolute cross sections were measured. Accordingly, it was necessary to detect small pulses in the Cerenkov counter and shower counter to ensure their efficiency. Only relative measurement were needed in this work so that only events with large pulses in both the shower counter and Cerenkov counter were included.

A lead filter of $\frac{1}{2}$" Pb (3 radiation lengths) was inserted in the scattered beam near the target at each momentum setting of the spectrometer. With this thickness, no more than 1% of the electrons emerge with energies greater than one half of the incident energy; since we only studied electrons from half the elastic scattered energy upwards, this filter effectively removes the electrons. However, high energy pions are reduced by only 10%.

It was verified that this filter indeed leaves the pions by observing the background without the Cerenkov counter, or shower counter, or at a momentum setting above the elastic peak where only pions penetrating the shielding or scattering off the pole tips could count. The background was hardly affected by the presence of the filter. We were, therefore, able to show that the background of pions was always less than 10% of the total counts and usually close to zero. When we tried to observe excitation of the mass 1512 MeV resonance at $\theta=90^{\circ}$ and $q^2 = 1(\text{BeV}/c)^2$ the background as determined by the lead filter was too large and the attempt was abandoned.

Radiative Corrections

This has been called, in the past, the correction for wide angle bremsstrahlung. We prefer to regard it as part of a general radiative correction calculation.

Although the most thorough discussion of radiative processes is that of Bjorken[5], an easier procedure to follow is described by Perez-y-Jorba[6]. Experimentally we measure a cross section $\sigma_{\text{meas}}(E_i, E_f) = d^2\sigma/(d\Omega dE_f)$ for finding a scattered electron of energy E_f. We are interested in a hypothetical cross section which we would measure if there were no radiative processes. Electrons radiate both before and after scattering. Thus, $\sigma_{\text{meas}}(E_i, E_f)$ includes contributions from $\sigma_o(E_i, E_f')$ (where $E_f' > E_f$) weighted by a radiation kernel $K_A(E_f', E_f)$ for radiation of a photon of energy $E_f' - E_f$ (radiation after scattering). Similarly, there is a term in $\sigma_o(E_i', E_f)$ for $(E_i > E_i')$ which is due to radiation <u>before</u> scattering. There is also the usual Schwinger correction which corresponds to inelastic events $\sigma_o(E_i, E_f)$ with radiation out of the detector bin width Δ.

According to the Perez-y-Jorba recipe therefore,

$$\sigma_{measured}(E_i, E_f) = \sigma_o(E_i, E_f)\,(1 - \delta) + \int_0^{E_i - \Delta E} K_B(E_i E_i')\,\sigma_o(E_i', E_f)\,dE_i' + \int_{E_f+\Delta E}^{\infty} K_A(E_f', E_f)\,\sigma_o(E_i, E_f')\,dE_f' \qquad (8)$$

where $\sigma_o(E_i, E_f)$ is the cross section for scattering without radiating; $(1 - \delta)$ is the Schwinger correction term; K_B is the radiation kernel for radiation before scattering; K_A that for radiation after scattering. These K's are calculated in the peaking approximation using the formula developed by L. N. Hand[2].

Here δ is given by $\frac{2\alpha}{\pi}\left(\left(\ell n \frac{E_f}{\Delta E} - \frac{13}{12}\right)\left(\ell n \frac{q^2}{m^2} - 1\right) + \frac{17}{36}\right)$

$$K_A = \frac{E_i'}{E_i}\,\frac{\alpha}{\pi}\,\frac{1}{E_i - E_i'}\left\{\ell n \frac{q^2}{m^2} - 1 + \frac{(E_i - E_i')^2}{E_i^* - E_i'}\left(\ell n \frac{2E_i}{m} - \frac{1}{2}\,\ell n\left(1 + \frac{2E_i}{M}\right)\right)\right\} \qquad (9)$$

$$K_B = \frac{E_f}{E_f'}\,\frac{\alpha}{\pi}\,\frac{1}{E_f' - E_f}\left\{\ell n \frac{q^2}{m^2} - 1 + \frac{(E_f' - E_f)^2}{E_f'\,E_f}\left(\ell n \frac{2E_f}{m} - \frac{1}{2}\,\ell n\left(1 + \frac{2E_f}{M}\right)\right)\right\}$$

Here Δ is the bin width at the detector.

We must also add a small (5%) addition to K_A, K_B and δ for

the real physical radiators present in the experiment.

Thus to evaluate the corrected cross section $\sigma_o(E_i, E_f)$ we must know $\sigma_o(E_i, E_f')$ at all values of E_f' from E_f up to the elastic scattering value and $\sigma_o(E_i', E_f)$ at all values of E_1' from E_i down to the elastic scattering value. The correction thus becomes an iterative procedure.

This is made clear by reference to Fig. (5). This is a kinematic diagram of the incident energy versus the scattered energy. Clearly, all elastic scattering events lie on a line on this plot. Inelastic events all lie to the left of this line - with smaller E_f.

When we consider the determination of the correction for a point, E_i, E_f in this plot, we see that the line integrals of Eq. (8) are the horizontal and vertical lines in this figure. Now, since we need to know $\sigma_o(E_i, E_f)$ at every point on the line, we see we must know $\sigma_{meas}(E_i, E_f)$ at all points in the shaded region before we may start the iteration.

$\sigma_o(E_i, E_f)$ is clearly known for elastic scattering by using the form factors from Ref. (3); for inelastic scattering it may be determined at any momentum transfer and K using data for lower momentum transfers and lower K. For the evaluation we must

interpolate between known points. This is done using Eq. (1) for the inelastic or elastic scattering and interpolating the elastic form factors according to Ref. (2) and the inelastic cross section σ_T according to the formula $G_{MV}^2(q)^{2\ell}$ where the value of ℓ is chosen from the two known points at the end of the interpolation range. This procedure approximates the expected theoretical behaviour of the cross section.

The radiative corrections have been evaluated using different bin sizes Δ; and using slightly different radiation kernals K_A, K_B. The results are insignificantly different.

Attempts were made to calculate the radiative correction according to the recipe of Bjorken[5]. However, the results gave $\sigma_o \simeq 1.1\ \sigma_{meas}$ contrary to physical intuition and to the Perez-y-Jorba calculation which gives $\sigma_o \simeq 0.9\ \sigma_{meas}$. The two methods should be equivalent (see Appendix I) though that of Bjorken is harder to apply. We feel that our attempts to calculate with the Bjorken recipe were subject to an unknown source of error and should therefore be ignored.

TREATMENT OF DATA

Two principal subtractions are to be made on the raw data viz., target wall scattering and the radiative corrections. Subtraction of detected pions in the scattereed beam was carried out by the lead filter technique described above and was always small. Electrons arising from charge symmetric processes (e.g., Dalitz pairs) were subtracted off by observing the positron cross section at various points along the spectra. This subtraction was also small. The subtracted counts had to be corrected for the shower counter efficiency at the particular bias and energy of the electron. These efficiencies were measured by observing the shower counter spectrum for elastically scattered electrons at comparable energies.

False kinematic coincidences such as that diagrammed in Fig. (6) were suppressed by demanding a signal from one of the slat counters.

The recipe followed then was:

1. To obtain the counts from hydrogen alone after wall subtraction.
2. To subtract counts with the field reversed.
3. To correct for background pions using the lead filter.
4. To normalize the inelastic counting rates to an absolute cross section by comparing them with the elastic counting

rate

5. To correct for shower counter efficiency

6. To compute the radiative corrections

Target Wall Background

The fraction of electrons scattered from the target wall varied from 10% to 20% of the total scattering. This fraction was determined by measuring the distribution of the beam across the target using the beam clipper as described in Ref. (3); from this we deduce directly the fraction of bremsstrahlung from the hydrogen, G. The calculation then proceeds as follows.

Let N be the number of counts for a given run, Q the charge collected by the quantameter and R=N/Q the counts per unit charge. More precisely, let N_H^- equal the number of positron counts in the reversed field subtraction, N_H^+ equal the number of positron counts in the reversed field runs. Let $N_M^{\pm}$ be similarly defined for the Mylar cup of the H-film (target wall scattering). Let Q_H equal the quantameter charge due to bremsstrahlung in the hydrogen, let Q_M be the same for the target wall. Let $G = \frac{Q_H}{Q_H+Q_M}$ be the fraction of bremsstrahlung for H_2.

This G is obtained from a knowledge of the shape of the

target cup and measurements of the amount of bremsstrahlung as a function of the amount of target exposed to the beam.

Note then that the raw counting rate R_o is given by:

$$R_o = \frac{N_H^- + N_H^+ + N_M^- + N_M^+}{Q_H + Q_M} \qquad 10$$

The counting rate from the solid target (of the same material as the target wall were ~~alone is~~ also measured.

$$R_M = \frac{N_M^- + N_M^+}{Q_M} \qquad 11$$

this should be the same number for the target wall alone.

And the reversed field for H_2 plus target wall

$$R_o^+ = \frac{N_H^+ + N_M^+}{Q_H + Q_M} \qquad 12$$

And the reversed field for the target wall alone is

$$R_M^+ = N_M^+/Q_M \qquad 13$$

The number that is wanted is

$$R_H^- = N_H^-/Q_H \qquad 14$$

Solving for this in terms of the measured quantities, we obtain

$$R_H^- = \frac{1}{G}\left(\left[R_o - R_o^+\right] - (1 - G)\left[R_M - R_M^+\right]\right) \qquad 15$$

Consider the two limiting cases:

$$A)\quad R_M^+ = 0,\quad R_H^- = \frac{1}{G}\left(R_o - \left[1 - G\right]R_M\right) - R_o^+/G \qquad 16$$

$$B)\quad R_M^+ = R_H^+,\quad R_H^- = \frac{1}{G}\left(R_o - \left[1 - G\right]R_M\right) - R_o^+ \qquad 17$$

In practice there is not much difference since R_o^+ is always about 5% or less of R_o.

The correction is listed as a multiplicative correction and includes the correction to the monitoring as well as that due to scatter from the walls. This somewhat disguises its real form which we therefore now discuss. From Eq. (17) we note that when G=0.9 (90% of the bremsstrahlung from hydrogen which is true for E =5 BeV) and $R_M=R_o$, we have 10% of the scatters due to the target walls yet the multiplicative correction is near unity. The correction differs from unity when the fraction of events scattered from the target walls is different from the fraction of the bremsstrahlung from the walls.

Absolute Normalization

The data was taken in such a way that absolute cross sections were obtained. In this paper we do not discuss the details of solid

angle determination, monitoring, etc. which are fully treated in Ref. (3). For convenience, the data consisting of a set of values of R were normalized to the elastic cross sections measured in Ref. (2) by the formula:

$$\frac{d^2\sigma}{d\Omega dE_f} = \left(\frac{d\sigma}{d\Omega}\right)_{\substack{\text{elastic} \\ \text{(Ref. 2)}}} \frac{R_{inel}}{R_{el}} \frac{1}{\Delta E_f} \qquad 18$$

where ΔE_f is the bin width.

DATA

The data are presented in Tables I, II, and III at incident energies (E_i) of 2.358, 2.988 and 4.874 BeV respectively. The laboratory scattering angle (θ) is 31° in each case.

The column headed E_f contains the values of the scattered energy at which electrons were detected. This scattered energy, E_f, is the central energy of the detection bin. The actual bin widths were .0157, .0146 and .0144 times E_f for Tables I, II and III respectively. For each table, the third entry for E_f is the elastic scattered energy.

The column headed R contains the observed counting rate,

electron events per quantameter count, for electrons scattered from the hydrogen filled mylar cup.

The column headed ST contains the correction factor to be applied because of target cup scattering. It is computed, using Eq. (15) and is equal to R_H^-/R_o.

The column headed RAD contains the correction factor to be applied because of radiative corrections. This is computed using the Perez-y-Jorba recipe and is equal to $\sigma_o/\sigma_{observed}$. In practice, the data for σ_{obs} was graphically smoothed and thus interpolated for equally spaced values of E_f, viz. ΔE_f .020 BeV. This value of ΔE_f was about the same size as the bin width, and was small enough to show the structure of the resonances. Then for each of these values of E_f, the correction factor σ_o/σ_{obs} was obtained and this factor was then interpolated (linearly) to the actual value of E_f that appears in the E_f column.

The column headed σ_o contains the final value of the non-radiative inelastic cross section $\frac{d^2\sigma}{d\Omega dE_f}$ and is expressed in 10^{-32} cm^2/BeV - Steradian.

The column headed Δ contains ~~the percent standard deviation for Poisson distributions, i.e., $1/\sqrt{n}$~~, the statistical error in percent. These are listed separately from the systematic errors

so that the shape of the spectrum can be easily seen.

The following systematic errors also appear. These, however, will not produce spurious peaks.

For the radiative corrections, we expect the error to vary from 5% for the 1238 resonance to about 15% for the most inelastic regions. The error comes from the peaking approximation used and we have estimated pessimistically the uncertainty at the higher resonances since the correction depends on previously corrected data and also on interpolated corrected data.

An error of 5% is assigned to the type of energy bin width determination as discussed near Eq. (16-a) viz., the overlapping of the slat counters.

The uncertainty resulting from the hysteresis of the magnet is less than 1%.

The remaining contribution to the systematic error is the uncertainty in the measured elastic cross section sections used to normalize the inelastic data. These were given as 8%, 8.5%, and 14% for E_i = 2.358, 2.988, and 4.874 BeV, yielding for the total systematic errors 11% to 18%, 11% to 18% and 16% to 22%.

Normalizing factors (cf. Eq. (18)) were found to be conveniently expressed as $F=\left.\frac{d\sigma}{d\Omega}\right|_{obs} \times \frac{1}{R_{el} wE_f}$ where $wE_f=\Delta E_f$. The values of F are $\frac{21.4}{E_f}$, $\frac{6.21}{E_f}$, and $\frac{57.9}{E_f}$ respectively.

An additional error of at most 0.3% was introduced into the bin width by averaging over the five slats after a given energy bin was centered on each in turn, because the tilt of the slat counters to the perpendicular to the magnet axis was neglected and because the dispersion in energy was approximated by a constant, viz. $\frac{\Delta E_f}{E_f} = .00718$ per inch.

This value of $\frac{\Delta E_f}{E_f}$ per inch was the average for the dispersion through a distance of six inches centered about the central slat and was the same for effective lengths of the magnet of 54, 53 and 52 inches.

That the effect of this error on the resolution function is negligible can easily be seen by superimposing five resolution functions, each similar to Fig. (4) and displaced one after the other by .15%.

Figures (7), (8), and (9) show the differential cross sections as functions of scattered energy for incident energies of 2.358, 2.988 and 4.874 BeV respectively and scattering angles of 31°

before radiative corrections have been made, i.e. only the ~~solid~~ wall target corrections have been applied. The radiative correction, in the form $(\sigma_{observed} - \sigma_{non\text{-}radiative})$ is represented by the dotted line.

The G factor, as used in Eq. (16) for the target wall scattering correction had the values 0.670, 0.760, and 0.890 for the three incident energies respectively.

Other data, shown in Table IV were taken including the M^*=1238 MeV resonance only both at 31° and at 90°. These are presented as averages over the resonance; averaged over an interval ΔK=150 MeV, centered on K=325 MeV.

Excitation of the M^*=1238 resonance

The most obvious feature of the scattered electron spectra, after the elastic scattering itself, is the peak at the mass M^*=1238 MeV. This is well known, has been the object of previous studies and will now be discussed. A treatment based on relativistic dispersion relations of the photoproduction of this resonance was first presented by Chew, Goldberger, Low and Nambu[7] (CGLN). This

was later extended to electroproduction by Fubini, Nambu and Watagin[8] (FNW) and further refined by Zagury[9] and Adler[10].

The CGLN theory assumes that the (3, 3) resonance dominates the dispersion integrals and the resonance position is taken from experiment. Then an effective range relation is obtained for the resonant P phase shift and the small S, D and non-resonant P phases are derived. The theory was applied firstly to π^- (pion-) nucleon scattering and then to photoproduction. FNW, using a static model, extended the theory to electroproduction.

In its simple form, the theory had only a qualitative success. A modified form was first used by Hand[2]. Hand recognized that the relation between pion nucleon scattering and photoproduction is more definite than other features of the theory and took pion nucleon phases from the experiment. Thereby, he achieved the first good success of the theory in fitting the total cross sections with no free parameters.

More recently Höhler[11] has retained the Born terms and the resonant amplitude and neglected the contribution of the small phases which calculation was in any case open to question. He obtained good fits to differential cross section and polarization data, except near $\theta=0^{\circ}$ where the small terms are important. Adler follows

the treatment of Höhler and extends it to electroproduction. The results are equivalent to those of Hand, but he uses a better approximation for electroproduction than the static model of FNW and his results differ slightly at high momentum transfers.

The relation between photoproduction and pion nucleon scattering inherent in CGLN and exploited by Hand, Höhler and now Zagury and Adler, was foreshadowed in a theorem due to Fermi and Watson that the phase of the photoproduction amplitude must be the same as that of the pion nucleon scattering amplitude until inelastic channels in the scattering open up. This holds only for the first (M = 1238 MeV) resonance; the higher resonances show great inelasticity and an equivalent relation has not been found.

The isobar model of Gourdin and Salin[12], extended to photoproduction by Loubaton[13] is superficially different. The results are, however, equivalent. The model automatically satisfies the Fermi-Watson theorem and the parameters are fitted to pion nucleon scattering. Likewise, inelasticity limits its usefulness to the first resonance.

An examination of the equations of FNW show that the dominant part of the electroproduction amplitude is indeed the resonant (3, 3) term. The principal variation is according to the formula,

$$\sigma_T \propto \left[G_{MV}\ (q^2)\right]^2 \left|\vec{q}\right|^2 \qquad 19$$

with a slight fall off at higher momentum transfers. (It is in the details of this fall off that Adler and Zagury improve on FNW.)

Now $G_{MV}(q^2)$ is not completely determined. Although $G_{Mp}(q^2)$ is measured by the elastic cross sections concomitant to this experiment, $G_{Mn}(q^2)$ is quite poorly known at high momentum transfers. The best guess available is that the form factors are well approximated by a "4 pole fit"[14]. Some more recent elastic electron-proton data[15] suggest that G_{Mp} may be lower than suggested by this 4-pole fit.

Figures (10), (11), and (12) show the absolute differential

cross sections for the resonance $M^* = 1238$ MeV compared to Adler's theory. (Adler and Zagury agree so it is only necessary to compare to one of them). The data lie 30% to 100% above the calculated curve - a fact already noted by Hand[2] at lower momentum transfers. However, we consider agreement to this accuracy at these high momentum transfers as a remarkable triumph of theory.

There seems to be a shift in the position of the peak towards higher values of M^* from the 1220 MeV predicted by the theory (the theoretical peak is <u>not</u> at the mass 1238 MeV). This shift is about $2\frac{1}{2}\%$ in M^* and we believe it is largely real. The magnet calibration was checked (to better than 0.5%) with elastic scattering (M=938 MeV) and we believe the magnet's effective length and field gradient to be reproducible to 0.4% and 0.3% respectively as functions of the magnet current.

We could interpret the comparison of theory and experiment as a measure of $\left(G_{MN}(q^2)\right)^2$. From what we have just said $\left(G_{MV}(q^2)\right)^2$ must be raised by 30% and $G_{MV}(q^2)$ by 15% to fit the data. Since

$G_{Mp}(q^2)$ is fixed, G_{Mn} must be increased 30% from the 4-pole fit. The theories all predict that there is no electric quadrupole excitation of the resonance, but there is evidence for a 3 - 5% admixture of the electric quadrupole with the magnetic dipole excitation. This evidence comes from the angular distribution of recoil protons in π^o photoproduction at resonance using polarized photons[16] and the equivalent experiment with electron scattering, the angular distribution of the protons in coincidence with electrons scattered inelastically from protons exciting the resonance.

Associated with the electric quadrupole excitation must be some longitudinal excitation. This can be separated by an angular distribution method, just as G_E and G_M may be separated in elastic scattering.

Hand[2] already showed that $\sigma_0/\sigma_T < 0.3$ at $q^2=5$ f^{-2}. By use of our measurements at $\theta=90^o$ (Table IV), we can put upper limits on σ_0 as shown in Table V. We plot σ_0 and σ_T against q^2 in Fig. (13) and Fig. (14) together with the theory; ($\sigma_0=0$ and solid line for σ_T). Our data is nowhere near precise enough to find the expected value of σ_0 from the known electric quadrupole excitation.

General Theory of Resonance Excitation

Although the theory of excitation of the resonance at $M^* = 1238$ MeV is good, no such theory exists for higher resonances. In pion nucleon scattering, inelastic channels are open[18] and there is considerable inelasticity in the scattering amplitude. The Fermi-Watson theorem does not then apply and a dispersion theory such as that of CGLN cannot easily be justified.

Some general statements can, however, be made about the excitation of resonances. These are well known in the realm of nuclear physics and are extensively used.[19] We here refer to a review paper by Barber[19]. In the nuclear physics problem the approximation is usually made of no nuclear recoil (for elementary particles this is the static model). A multipole expansion may then be carried out in the laboratory reference frame. The results derived are valid in the long wavelength limit $qr \ll 1$ where r is the interaction radius - which is presumed to be of the order of the nuclear radius, r_o. In elementary particle physics the results derived in the long wavelength limit are sometimes called threshold conditions and we are usually far from $qr \ll 1$.

The calculation of σ_T involves the squared matrix element

$$\sigma_T \propto \left| \int \frac{j_\ell (qr)\ Y_{\ell 0} (\theta' \phi')\ \rho(r)}{\left| \underset{\sim}{q} \right|} d^3 r \right|^2 \qquad 20$$

where $\rho(r)$ is an interaction density which is non-zero only for $r < r_0$ and $\underset{\sim}{q}$ is the 3 dimensional momentum transfer.

The full calculation[19] yields for magnetic transitions of order ℓ (sometimes called abnormal parity transitions):

$$\sigma_T (q^2, K) = 4 \left(\frac{\vec{\underset{\sim}{q}}}{K} \right)^{2\ell} \sigma_\gamma (K)$$

$$\sigma_0 (q^2, K) = 0 \qquad 21$$

and for electric transitions of order ℓ (often called normal parity transitions) except monopole.

$$\sigma_T (q^2, K) = 4 \left(\frac{\underset{\sim}{q}}{K} \right)^{2\ell - 2} \sigma_\gamma (K)$$

$$\sigma_0 (q^2, K) = 4 \frac{\ell}{\ell + 1} \left| \frac{\underset{\sim}{q}}{K} \right|^{2\ell - 2} \frac{q^2}{K^2} \sigma_\gamma (K) \qquad 22$$

$$= \frac{\ell}{\ell + 1} \frac{q^2}{K^2} \sigma_T (q^2, K)$$

Bjorken and Walecka[20] derive similar formulae for σ_T including

nuclear recoil. However, they find:

$$\sigma_o (q^2, K) = \frac{\ell}{\ell + 1} \frac{q^2}{q_o^{*2}} \sigma_T (q^2, K) \qquad 23$$

In the static model and long wavelength limit this is the same as Eq. (21 because $q_o^* = K$ for $M^* \approx M$ and $q^2 = 0$.

We note the kinematical relationship:

$$\left|\underset{\sim}{q}^*\right| M^* = \left|\underset{\sim}{q}\right| M \qquad 24$$

This makes it immaterial which initial or final nucleon system reference frame we use for Eq. 21 and 22 provided K is measured in the same frame. At $q^2 = 0$

$$\left|\underset{\sim}{q}^*\right| / K^* = \left|\underset{\sim}{q}\right| / K = 1 \qquad 25$$

Eq. (23) depends on the following theorems: (Ref. 20)

$$\lim_{|\vec{q}^*| \to 0} L_{\ell-} / E_{\ell-} = - \frac{\ell - 1}{\ell} \quad \text{for } \ell \geq 2,$$

$$\lim_{|\vec{q}^*| \to 0} L_{\ell+} / E_{\ell+} = 1 \quad \text{for } \ell \geq 0$$

and

$$M_{\ell\pm} \to |\vec{q}^*|^{\ell} \text{ for } \ell \geq 1. \qquad 26$$

where $M_{\ell\pm}$, $E_{\ell\pm}$ and $L_{\ell\pm}$ are the magnetic, electric and longitudinal multipole coefficients respectively.

When $q_0^* = 0$, it can be shown that all the $L_{\ell\pm}$ vanish,[21] thus the $\frac{L}{E}$ behaviour for small $|\vec{q}^*|$ breaks down and it is not known what the theoretical ratio of $\sigma_{long}/\sigma_{trans}$ is.

For curiosity's sake, the ratios of $\sigma_{long}/\sigma_{trans} = \sigma_O/\sigma_T$ according to various prescriptions are given for three points of interest in Table VI. Likewise, the behaviour of q_o^2 and q_o^{*2} as functions of q^2 is shown in Fig. 15.

The formulae given above for the long wavelength limit (threshold condition) certainly do not apply to our case where $|q|\, r \sim 1$ (and do not even apply well for nuclear physics). One must multiply the Eq. (21) and (22) by some arbitrary form factor. At first sight, it is not clear that we have achieved anything by all this manoevring; we started with an arbitrary function $\sigma_T(q^2, K)$ and still have an arbitrary function $F^2(q^2, K)$. But the form factor is now expected to be characteristic of the nucleon size. If we refer back to Eq. (20)

we may guess the interaction density to be equal to the nucleon size. This may be approximated (Ref. (3)) by an exponential $e^{-\lambda r}$ which is the Fourier transform of the form factor:

$$F(q^2) \propto \left[\frac{1}{1 + q^2/(0.72)}\right]^2 \qquad 27$$

according to,

$$\left|\int j_o(qr)\, e^{-\lambda r}\, d^3r\right|^2 \propto \left|F(q^2)\right|^2 \qquad 28$$

For the magnetic dipole transition to $M^* = 1238$ MeV, for example, we find that

$$\left|\int j_1(qr)\, e^{-\lambda r}\, d^3r\right|^2 \propto q^2 \left|F(q^2)\right|^2 \qquad 29$$

The relevant form factor is clearly the magnetic vector form factor $G_{MV}(q^2)$ and we find therefore the recipe of Eq. (19) which we found earlier was the dominant term in the FNW dispersion theory calculation, but not including the kinematic factors included by Adler.

For the other resonances, the theory is less certain for many reasons. At the start of this work, resonances were known at $M^* = 1512$ MeV $(I = \frac{1}{2},\ J = \frac{3^-}{2})$ and $M^* = 1688$ MeV $(I = \frac{1}{2},\ J = \frac{5^+}{2})$ were

known from pion nucleon scattering and photoproduction. Since then, phase shift analyses of pion nucleon scattering[18] have shown the existence of other resonances superimposed at these energies. The disentanglement of their contributions to photoproduction has not been performed and it would be harder for electroproduction (for which there is less data). We shall proceed to analyse the data on the supposition of only these two (old) resonances - plus a background.- and endeavor to derive what information we can. As we shall see, no amount of contribution of the new resonances can affect a peculiarity of the excitation at $M^*=1512$ MeV.

Another uncertainty is what form factor to use for these resonances. For a resonance dominated by transverse excitation the magnetic form factor is probably appropriate since the magnetic form factor is the name given to the transverse elastic form factor. But a transition to a state of $I=\frac{1}{2}$ should involve $G_{MS}(q^2)$ and not $G_{MV}(q^2)$. Now,

$$2\,G_{MS}(q^2) = G_{Mp}(q^2) + G_{Mn}(q^2)$$

$$2\,G_{MV}(q^2) = G_{Mp}(q^2) - \left| G_{Mn}(q^2) \right| \qquad 30$$

G_{MS} therefore involves a subtraction of two numbers of the same

order of magnitude and is very poorly known. For the longitudinal excitation to $I = \frac{1}{2}$ state, probably $G'_{ES}(q)$ becomes important and the electric form factors are hardly known at all at the momentum transfers of interest here. For the sake of definiteness and for no other reason, we have chosen to compare our results to $G_{MV}(q^2)$ as for the $M^* = 1238$ MeV case. Table VII shows how the form factors G_{MV} and G_{EV} might change for two fits which are not far from known data (but note that at $q^2 \sim 4(\text{BeV/c})^2$ the 1-parameter fit (Eq. 27) does not fit the data to which this experiment is normalized.)

Breit-Wigner Fits and Multipole Fits

The problem arises ~~how much is~~ of the size of the resonant contribution ~~and how much is~~ relative to the non-resonant contribution. For the first resonance there is enough understanding to know that $\frac{1}{4}$ of the photoproduction cross section at the peak is non-resonant. We can see this most easily from the statement that the transition $\gamma + P \rightarrow P + \pi^0$ is entirely resonant, and from Clebsch-Gordan coefficients is twice the resonant cross section in $\gamma + P \rightarrow n + \pi^+$. Yet these two cross sections are experimentally equal, hence there

is a non-resonant background in $\gamma + P \rightarrow n + \pi^+$ equal to $\frac{1}{4}$ of the total γ absorption cross section.

The non-resonant part falls somewhat faster with increasing momentum transfer than the resonant part and probably is small at $q^2 = 90\ f^{-2}$. In the detailed comparison with theory made earlier for the first resonance, the non-resonant background is, of course, included.

The crude separation of the resonances discussed below is based on the assumption that the widths remain the same as the value at $q^2 = 0$, and is therefore somewhat arbitrary. In view of these reservations, and those discussed earlier, we still endeavor to make some physical interpretation of the data.

After the radiative corrections were carried out by the Perez-y-Jorba method, the resonant part of the scattering was estimated from the shapes of the resonances. In trying to determine whether or not a resonance exists, only the statistical errors in Figs. (16), (17), and (18) are significant because the radiative, solid target, and shower efficiency corrections give smooth curves. The full width at half height was calculated a priori, for each of the four resonances, ($N^*(1238)$, $N^*(1512)$, $N^*(1688)$, and $N^*(1920)$ and for each of the three incident

energies, (2.358, 2.988 and 4.874 BeV) assuming widths of 130, 140, 145, and 185 MeV respectively.

The scattered energies and widths at which these resonances were expected to be observed were calculated from kinematics. To these were added in quadrature the width of the elastic peak (i.e., at corresponding incident energies) to obtain the expected experimental width of each resonance at each incident energy.

Half of the resonant contribution was then assumed to be the difference between the cross section at the peak of the resonance and the average of the cross section, a half-width either side of the peak. These amplitudes are shown in Table VIII. The crudeness of this method introduces large uncertainties which have been estimated to be anywhere from a factor of $1\frac{1}{4}$ to a factor of 4 depending on how clearly the resonance stands out.

If we assume a resonant structure of the form:

$$\left.\frac{d^2\sigma}{dE_f d\Omega}\right|_{\text{resonant}} = \frac{A\ \Gamma^2/4}{(E_f - E_{res})^2 + \Gamma^2/4} \qquad 31$$

we find the average from $E_{res} - \frac{\Gamma}{2}$ to $E_{res} + \frac{\Gamma}{2}$ to be

$$\left.\frac{d\sigma}{d\Omega}\right|_{\text{resonant}} \div \Gamma_{E_f} = \frac{\pi}{4} A \qquad 32$$

This permits us to use the peak amplitude in estimating the multipole fits.

The non-resonant contribution to the scattering was then assumed to be what was left after the contributions of the four resonances were removed. Figs. (16), (17), and (18) show the inelastic spectrum after radiative corrections (the points with the bars), the contribution of each resonance (smooth bell shaped curves), the assumed non-resonant scattering (dotted line), and the reconstructed spectrum, i.e., the sum of the assumed non-resonant and of all four resonances (single smooth line).

Fig. (19) shows the total cross section for photoproduction as compiled from the data for:

$$\begin{aligned}
P + \gamma &\rightarrow P + \pi^0 \\
&\rightarrow n + \pi^+ \\
&\rightarrow P + \pi^+ + \pi^- \\
&\rightarrow P + \pi^+ + \pi^- + \pi^0 + (\gamma\pi^0) \\
&\rightarrow n + \pi^+ + \pi^+ + \pi^- + (\gamma\pi^0) \\
&\rightarrow P + 2\pi^+ + 2\pi^- + (\gamma\pi^0) \\
&\rightarrow n + 3\pi^+ + 2\pi^- \\
&\rightarrow \text{strange particles}
\end{aligned}$$

For some purposes it is more convenient to use the cross section integrated over the resonance, i.e., $\left.\frac{d\sigma}{d\Omega}\right|_{\text{over resonance}}$

Accordingly the values of

$$\int_{-\infty}^{\infty} \frac{A\Gamma^2/4}{(E_f - E_{res})^2 + \Gamma^2/4}\, dE_f = \frac{\pi}{2} A \qquad 33$$

are given in Table IX.

The values of σ_T used in the multipole fits were obtained from the data in Table VIII and the following formulas:

For $N^*(1238)$ and $N^*(1920)$, according to Eq. (1) and the rule stated after Eq. (23),

$$\frac{d^2\sigma}{d\Omega dE_f} = \sigma_T (q^2, K)\, \Gamma_T (\theta, q^2, K) \qquad 34$$

and for $N^*(1512)$ and $N^*(1688)$, according to Eq. (1) and (23)

$$\frac{d^2\sigma}{d\Omega dE_f} = \sigma_T (q^2, K)\, \Gamma_T(\theta, q^2, K) + \frac{\ell}{\ell+1} \frac{q^2}{K^2} \Gamma_0(\theta, q^2, K) \qquad 35$$

where $\ell = 1$ or 2 for $N^*(1512)$ or $N^*(1688)$ respectively.

The values for σ_T (q^2, K) thus obtained are given in Table IX.

As a test of Eq. (21) and (22) the values of the logarithm of $\frac{\sigma_T}{G_{MV}^2}$ are plotted against the logarithm of $\left|\vec{q}^2\right|$ for constant M^*. The results are shown in Fig. (20), (21) and (22).

By reason of the previously indicated arguments about change in angular momenta, isotopic spin, and parity, we expect the excitation of the resonances to go as indicated by the dashed lines.

Comparison of these assignments with Fig. (20), (21) and (22) shows rather remarkable agreement considering the approximations that entered into the calculations. A possible deviation exists at 1512 where the electric dipole excitation prediction does not simultaneously fit the photoproduction and electroproduction data. The new resonances would be excited by electric monopole and dipole excitation. Possible reasons for the discrepancy are the replacement of q_0^* by K (use of Eq. (22) instead of (23)) and use of G_{MV} instead of G_{ES}.

Conclusions and Speculations

The excitation of the resonances at M^*=1238 MeV agrees reasonably with theory and further work can identify details. A separation of σ_0 and σ_T by measurements of this type or by the distributio

in the azimuthal angle ϕ of the outgoing protons can give information on the electric quadrupole admixtures as a function of momentum transfer.

Similar separation at the higher resonances should confirm the assumption that longitudinal transitions play an important role in the production of some of ~~the~~ these resonances.

It is interesting to speculate on the excitation of higher resonances. According to present ideas, these should be of high spin corresponding to Regge recurrences (rotational states) of the nucleon and the $M^*=1238$ MeV state. They should then stand out more strongly in electroproduction than photoproduction because of the factor $(\underset{\sim}{q}r)^{2\ell}$ in σ_T. But this increase has its limits; the relative enhancement in electroproduction should really be considered as a suppression of higher multipoles in photoproduction. When $qr \sim 1$ the threshold behaviour clearly breaks down. But a naive use of Eq. (20) suggests a relative enhancement of a factor of 20 for a $J=\frac{11}{2}$ resonance with mass 3 BeV for a momentum transfer of ~ 10 (BeV/c)^2.

The use of a high energy accelerator (e.g. SLAC) is clearly indicated for this study both for reaching the high momentum transfer and for reducing the radiative corrections.

ACKNOWLEDGEMENTS

Our thanks go to J. Chen who assisted in the detailed preparation of the paper.

Our thanks also go to the CEA staff for producing accelerated beams without which this work could not have been done*. The cyclotron laboratory staff** ably constructed the apparatus.

Much valuable assistance was provided by M. Goitein, R. Budnitz, K. Hanson, A. Liberman, and C. Mistretta.

*In particular we would like to acknowledge the assistance of Art Hansen and his crew and also the enthusiastic assistance of the operations group under Dr. G. Voss.

**Under the direction of M. Wanagel, J. McElaney, D. Wharton and W. Dunn.

APPENDIX

Radiative Corrections

Bjorken writes down a formula relating $\sigma_{meas}(E_i, E_f)$ and $\sigma_o(E_i, E_f)$:

$$\sigma_m(E_i, E_f) = \int_0^{E_i} dE_i' \int_{E_f}^{\infty} dE_f' \; P(E_i, E_i', \delta_i)\; \sigma_o(E_i', E_f')\; P(E_f', E_f, \delta_f) \qquad \text{A-1}$$

where $P(E,E',\delta)$ is the probability of an electron of energy E radiating to produce on of energy E' with radiator δ.

To include internal radiative effects in the peaking approximation

$$\delta_{i,f} = \frac{\alpha}{\pi} \left(\log (q^2/m^2) - 1\right) + t_{i,f} \Big| \log 2 \qquad \text{A-2}$$

where $t_{i,f}$ are the thickness of the physical radiators in the path of the incident (final) beam in radiation lengths.

Bjorken approximated:

$$P(E,E',\delta) = \frac{\left[\log (E/E')\right]^{\delta-1}}{E\,\Gamma(\delta)} = \frac{\delta}{E \log E/E'} \qquad \text{A-3}$$

for small δ.

Now replace $\int_0^{E_i}$ by $\int_0^{E_i-\Delta} + \int_{E_i-\Delta}^{E_i}$ and $\int_{E_f}^{\infty}$ by $\int_{E_f}^{E_f+\Delta} + \int_{E_f+\Delta}^{\infty}$,

where Δ is the bin size as in the Perez y Jorba recipe.

Then:

$$\sigma(E_i, E_f) = \int_{E_i-\Delta}^{E_i} dE_i' \int_{E_f}^{E_f+\Delta} dE_f' \; P\, \sigma_o\, P$$

$$+ \int_{o}^{E_i-\Delta} dE_i' \int_{E_f}^{E_f+\Delta} dE_f' \; P\, \sigma_o\, P$$

$$+ \int_{E_i-\Delta}^{E_i} dE_i' \int_{E_f+\Delta}^{\infty} dE_f' \; P\, \sigma_o\, P \qquad \text{A-4}$$

$$+ \int_{o}^{E_i-\Delta} \int_{E_f+\Delta}^{\infty} P\, \sigma_o\, P$$

Integrate over the interval Δ, and assume

$$\frac{\Delta}{E_{i,f}} \ll 1, \quad \delta \ll 1.$$

Note that

$$\int_{E_f}^{E_f+\Delta} dE_f' \; \frac{1}{E_f'} \; \frac{\left[\ell n\, E_f'/E_f\right]^{\delta_f - 1}}{\Gamma(\delta_f)} = \left(\frac{\Delta}{E_f}\right)^{\delta_f} \qquad \text{A-5}$$

$$= e^{\delta \ell n \frac{\Delta}{E_f}} = 1 + \delta_f \ell n \frac{\Delta}{E_f} + O(\delta^2)$$

and similarly:

$$\int_{E_i-\Delta}^{E_i} dE_i' \; \frac{1}{E_i} \; \frac{\left[\ell n\, E_i/E_i'\right]^{\delta_i - 1}}{\Gamma(\delta_i)} \simeq 1 + \delta_i \ell n \frac{\Delta}{E_i} + O(\delta^2)$$

Also note that:

$$\int_{E_f+\Delta}^{E_{fMAX}} \frac{dE_f'}{E_f'} \frac{\left[\ell n\, E_f'/E_f\right]^{\delta_f - 1}}{\Gamma(\delta_f)}$$

$$= \left(\ell n \frac{E_{fMAX}}{E_f}\right)^{\delta} - \left(\ell n \frac{E_f+\Delta}{E_f}\right)^{\delta} \qquad \text{A-7}$$

$$= e^{\delta \ell n (E_{fMAX}/E_f)} - e^{\delta \ell n\, \Delta/E_f}$$

$$= 1 + \delta \ell n \left(\ell n \frac{E_{fMAX}}{E_f}\right) + O(\delta^2) - \left[1 + \delta \ell n \frac{\Delta}{E_f} + O(\delta)^{-2}\right]$$

$$= \delta \left[\ell n \left(\ell n \frac{E_{fMAX}}{E_f}\right) - \ell n \frac{\Delta}{E_f} + O(\delta^2)\right.$$

Hence if we drop all terms in δ^2 and higher, we have

$$\sigma(E_i, E_f) \simeq \left(1 + 2\delta\, \ell n \frac{\Delta}{E_f}\right) \sigma_o(E_i, E_f)$$
$$+ \int_0^{E_i - \Delta} dE_i'\, P(E_i, E_i', \delta_i)\, \sigma_o(E_i', E_f) \qquad \text{A-8}$$
$$+ \int_{E_f+\Delta}^{\infty} dE_f'\, \sigma_o(E_i, E_f')\, P(E_f', E_f, \delta_f).$$

This shows that to first order in α the Perez y Jorba recipe is equivalent to the Bjorken recipe.

We note here that an additional calculation using the Perez y Jorba recipe with a bin size $\Delta E = .01$ BeV gave the same results as the calculation with $\Delta E = .02$ BeV.

We also note that a calculation using the Perez y Jorba recipe with Bjorken's radiation kernels instead of Hand's give corrected cross sections which differ by less than 1% from the quoted results. A comparison of the radiation kernels for the two cases (Table A-I) show that the differences are unimportant. At first sight, the difference of the Bjorken recipe in the first line seems inconsistent with equation A-8 and the statement derived therefrom. In Eq. (A-8) the approximation is made $\delta \ll 1$ which is valid when E' is close to E.

REFERENCES

1. W.K.H. Panofsky and E. Allton, Phys. Rev. 110, 1155 (1958).
2. L.N. Hand, Phys. Rev. 129, 1834 (1963).
3. K.W. Chen, J. R. Dunning, A. A. Cone, N. F. Ramsey, J. K. Walker, and Richard Wilson, Phys. Rev. 141, 1267 (1966).
4. J. R. Dunning, K. W. Chen, A.A. Cone, G. Hartwig, N. F. Ramsey, J. K. Walker, Richard Wilson, Phys. Rev. 141, 1286 (1966).
5. J. S. Bjorken, Ann. Phys. (N.Y.) 24, 201 (1963).
6. J. Perez y Jorba, Orsay Report No. 1108 (1964).
7. G. F. Chew, M.L. Goldberg, F. E. Low and Y. Nambu, Phys. Rev. 106, 1345 (1957).
8. S. Fubini, Y. Nambu and V. Wataghin, Phys. Rev. 111, 329 (1958).
9. N. Zagury, Phys. Rev. 145, 1112 (1966).
10. S. Adler, Proceedings, Argonne Conference on Weak Interactions (1965).
11. G. Hohler and W. Schmidt, Ann. Phys. (N.Y.) 28, 34 (1964).
12. M. Gourdin and Ph. Salin, Nuovo Cimento 27, 193, 309 (1963).
13. J. P. Loubaton, Nuovo Cimento 39, 591 (1965).
14. L. H. Chan, K. W. Chen, J. R. Dunning, N. F. Ramsey, J. K. Walker and Richard Wilson, Phys. Rev. 141, 1298 (1966).
15. Reports by DESY Groups to International Conference on High Energy Physics, Berkeley (1966).
16. R. C. Smith and R. Mozley, Phys. Rev. 130, 2429 (1963).
17. C. W. Akerlof, W. W. Ash, K. Berkelman and M. Tigner, Phys. Rev. Letters 14, 1036 (1965).

REFERENCES

18. A. Donnachi, A.T. Lea, C. Lovelace, Phys. Letters 19, 146 (1965).

19. W. C. Barber, Ann. Rev. Nucl. Sci. 12, 1 (1962).

20. J. D. Bjorken and J. D. Walecka, Ann. Phys. (N.Y.) 38, 35 (1966).

21. S. Adler (private communication).

Table I

$E_i = 2.358$ BeV

E_f	R	ST	RAD	σ_0	Δ
1.774	0.213	1.27			
1.754	0.598	1.40			
1.735	0.862	1.43			
1.716	0.485	1.38			
1.698	0.160	1.17			
1.680	0.119	1.04			
1.662	0.084	0.83	RAD	σ_0	Δ
1.643	0.0758	0.745	0.350	0.260	10
1.624	0.0955	0.881	0.398	0.446	14
1.607	0.0800	0.744	0.652	0.523	14
1.591	0.109	0.928	0.833	1.155	12
1.573	0.116	0.948	0.938	1.435	12
1.556	0.145	1.046	1.027	2.187	11
1.539	0.189	1.142	1.072	3.295	10
1.522	0.236	1.204	1.045	4.267	8
1.506	0.293	1.254	1.078	5.813	7
1.490	0.277	1.234	1.072	5.436	7
1.473	0.352	1.284	1.018	6.904	6
1.457	0.274	1.222	0.937	4.756	6
1.441	0.230	1.171	0.993	4.104	6
1.426	0.233	0.977	0.920	3.286	7
1.411	0.203	1.200	0.894	3.440	7

Table I (Cont.)

E_f	R	ST	RAD	σ_o	Δ
1.395	0.213	1.106	0.880	3.322	7
1.380	0.208	1.026	0.881	3.049	7
1.365	0.194	1.122	0.879	3.126	8
1.350	0.196	1.187	0.885	3.454	8
1.336	0.207	1.032	0.900	3.255	7
1.321	0.194	1.344	0.891	3.970	7
1.307	0.225	0.991	0.906	3.501	7
1.292	0.201	1.252	0.915	4.023	7
1.279	0.219	1.078	0.928	3.919	7
1.265	0.209	1.196	0.921	4.165	7
1.250	0.219	1.351	0.936	5.054	7
1.237	0.249	1.141	0.950	4.982	6
1.223	0.241	1.412	0.945	6.019	5
1.210	0.279	1.125	0.953	5.720	5
1.197	0.262	1.188	0.947	5.717	4
1.184	0.259	1.275	0.953	6.221	4
1.117	0.273	1.142	0.932	5.830	4
1.158	0.260	1.079	0.892	5.110	4
1.146	0.239	1.133	0.911	5.120	4
1.134	0.232	1.157	0.874	4.954	4
1.121	0.231	1.064	0.888	4.686	4
1.109	0.215	1.150	0.862	4.669	5

Table I (Cont.)

E_f	R	ST	RAD	σ_0	Δ
1.097	0.216	1.103	0.861	4.564	5
1.085	0.209	1.164	0.858	4.753	5
1.074	0.212	1.114	0.873	4.797	5
1.106	0.207	1.446	0.863	6.154	5
1.050	0.254	1.080	0.889	5.464	4
1.039	0.239	1.238	0.889	6.022	4
1.027	0.255	1.092	0.896	5.851	4
1.016	0.245	1.110	0.842	5.490	4
1.005	0.242	1.267	0.874	6.576	4
0.994	0.283	1.076	0.862	5.690	4
0.983	0.283	1.005	0.837	5.237	4
0.973	0.270	1.150	0.867	6.002	4
0.962	0.288	1.052	0.874	5.976	4
0.952	0.283	1.033	0.857	5.730	4
0.942	0.275	1.037	0.862	5.720	4
0.931	0.271	0.828	0.847	4.478	5
0.922	0.231	1.019	0.852	4.790	4
0.912	0.239	1.090	0.833	5.251	5
0.901	0.255	0.947	0.841	5.002	6
0.891	0.243	0.954	0.818	4.733	7
0.882	0.236	1.126	0.826	5.555	7
0.872	0.259	0.959	0.802	5.121	7
0.863	0.248	1.116	0.809	5.831	7

Table I (Cont.)

E_f	R	ST	RAD	σ_0	Δ
0.853	0.268	0.673	0.789	3.757	7
0.844	0.203	1.026	0.794	4.421	7
0.835	0.221	0.919	0.776	4.285	7
0.826	0.219	0.760	0.781	3.575	7
0.817	0.194	0.971	0.764	4.017	7
0.808	0.209	0.838	0.769	3.816	7
0.799	0.200	0.982	0.752	4.252	8
0.790	0.215	0.969	0.757	4.615	8
0.782	0.223	0.753	0.761	3.801	7
0.774	0.196	1.092	0.743	4.480	7
0.765	0.227	0.699	0.749	3.650	7
0.757	0.190	0.831	0.732	3.610	7
0.748	0.190	0.657	0.736	2.918	8
0.740	0.167	0.762	0.716	2.953	8
0.732	0.169	1.114	0.722	4.482	8
0.724	0.211	0.728	0.727	3.729	8
0.716	0.186	0.882	0.707	3.948	8
0.709	0.193	0.886	0.711	4.198	8
0.701	0.196	0.782	0.716	3.864	8
0.693	0.184	1.076	0.697	4.941	8
0.686	0.212	0.738	0.701	3.996	8
0.679	0.183	0.756	0.681	3.480	8
0.671	0.169	0.763	0.686	3.335	8

Table I. (Cont.)

E_f	R	ST	RAD	σ_o	Δ
0.664	0.161	1.055	0.691	4.496	8
0.657	0.187	0.857	0.669	4.173	8
0.649	0.178	0.598	0.674	2.853	8
0.642	0.140	0.826	0.679	3.178	9
0.635	0.145	0.988	0.657	3.855	9
0.628	0.161	0.858	0.662	3.822	9
0.622	0.157	0.911	0.666	4.039	9
0.615	0.158	0.808	0.640	3.528	9
0.608	0.146	0.766	0.646	3.179	9
0.602	0.133	0.804	0.652	3.131	9
0.595	0.129	1.200	0.616	4.339	9
0.589	0.159	0.765	0.624	3.522	9
0.582	0.135	0.641	0.633	2.596	9
0.576	0.110	1.222	0.587	3.825	10
0.570	0.140	0.895	0.596	3.701	10
0.563	0.133	0.691	0.605	2.805	10
0.557	0.108	1.269	0.555	3.938	10

Table II

$E_i = 2.988$ BeV

E_f	R	ST	RAD	σ_o	Δ
2.098	0.202	1.135			
2.076	0.630	1.252			
2.054	0.877	1.268			
2.032	0.644	1.249			
2.010	0.334	1.169			
1.988	0.191	1.044			
1.966	0.154	0.960			
1.945	0.131	0.876			
1.924	0.101	0.706	RAD	σ_o	Δ
1.904	0.074	0.953	0.468	0.255	13
1.883	0.216	1.006	0.860	0.622	7
1.863	0.286	1.075	0.991	1.025	6
1.843	0.381	1.128	1.062	1.55	5
1.823	0.464	1.156	1.083	1.99	4
1.803	0.465	1.151	1.072	1.99	3
1.783	0.405	1.121	1.027	1.65	4
1.764	0.401	1.114	0.972	1.55	4
1.745	0.390	1.103	0.930	1.44	4
1.726	0.339	1.063	0.909	1.19	4
1.707	0.373	1.080	0.905	1.34	4
1.688	0.372	1.074	0.904	1.35	4
1.670	0.388	1.078	0.916	1.45	4

Table II (Cont.)

E_f	R	ST	RAD	σ_3	Δ
1.652	0.393	1.076	0.928	1.49	4
1.634	0.413	1.083	0.937	1.62	4
1.617	0.428	1.087	0.943	1.71	4
1.599	0.428	1.083	0.956	1.78	4
1.581	0.508	1.115	0.914	2.14	4
1.156	0.541	1.124	0.960	2.36	4
1.547	0.576	1.133	0.980	2.62	4
1.531	0.656	1.152	0.984	3.08	3
1.515	0.650	1.148	0.951	2.98	3
1.498	0.567	1.120	0.907	2.45	3
1.481	0.588	1.126	0.940	2.68	3
1.465	0.548	1.108	0.897	2.37	3
1.449	0.522	1.097	0.878	2.21	3
1.433	0.561	1.108	0.872	2.42	3
1.418	0.559	1.105	0.882	2.46	3
1.403	0.548	1.110	0.872	2.40	3
1.388	0.561	1.110	0.889	2.53	3
1.372	0.629	1.123	0.901	2197	3
1.357	0.639	1.124	0.905	3.08	3
1.342	0.667	1.129	0.904	3.27	3
1.328	0.625	1.116	0.903	3.05	3
1.314	0.684	1.130	0.892	3.38	3
1.300	0.682	1.129	0.875	3.34	3

Table II (Cont.)

E_f	R	ST	RAD	σ_o	Δ
1.286	0.647	1.116	0.884	3.22	3
1.272	0.679	1.124	0.859	3.34	3
1.258	0.611	1.102	0.832	2.88	3
1.244	0.601	1.096	0.845	2.89	3
1.231	0.609	1.098	0.820	2.88	3
1.217	0.579	1.085	0.809	2.72	3.5
1.204	0.577	1.082	0.811	2.75	3.5
1.191	0.556	1.072	0.804	2.64	3.5
1.178	0.574	1.077	0.794	2.73	4.0
1.165	0.575	1.075	0.799	2.78	4.0
1.152	0.568	1.069	0.786	2.72	4.8
1.140	0.563	1.065	0.774	2.68	5.5
1.128	0.562	1.061	0.778	2.71	5.5
1.115	0.528	1.043	0.764	2.49	5.5
1.103	0.600	1.074	0.772	2.99	6
1.091	0.557	1.054	0.755	2.68	6
1.079	0.577	1.063	0.733	2.75	6
1.068	0.557	1.051	0.743	2.69	5.2
1.056	0.557	1.050	0.721	2.65	5.2
1.045	0.532	1.036	0.729	2.56	5.2
1.033	0.496	1.013	0.707	2.39	5.5
1.022	0.556	1.046	0.717	2.72	5.5
1.011	0.545	1.039	0.690	2.59	5.5

Table II (Cont.)

E_f	R	ST	RAD	σ_o	Δ
1.000	0.533	1.030	0.659	2.45	5.5
0.989	0.488	1.002	0.671	2.25	6
0.978	0.503	1.025	0.647	2.30	6
0.967	0.483	0.995	0.654	2.20	6
0.957	0.487	0.995	0.645	2.21	6
0.947	0.500	0.998	0.645	2.31	6
0.937	0.500	0.993	0.637	2.30	6
0.927	0.450	0.952	0.642	2.03	6
0.917	0.460	0.956	0.621	2.04	6
0.907	0.487	0.973	0.630	2.27	6
0.897	0.433	0.927	0.603	1.85	6
0.887	0.533	0.998	0.612	2.55	6
0.877	0.472	0.956	0.576	2.06	6
0.867	0.517	0.985	0.590	2.42	6
0.858	0.472	0.951	0.538	1.97	6
0.849	0.437	0.919	0.555	1.85	6
0.840	0.487	0.958	0.502	1.98	6
0.831	0.430	0.908	0.517	1.73	6
0.822	0.425	0.901	0.531	1.78	6
0.813	0.393	0.864	0.476	1.44	6
0.804	0.403	0.872	0.494	1.57	6
0.795	0.438	0.938	0.436	1.65	6
0.786	0.393	0.855	0.451	1.42	6

Table II (Cont.)

E_f	R	ST	RAD	σ_o	Δ
0.778	0.443	0.905	0.400	1.55	6
0.770	0.380	0.837	0.412	1.23	6
0.761	0.373	0.825	0.426	1.29	6
0.753	0.377	0.826	0.379	1.19	6

E_i = 4.874 BeV*

Table III*

Multiplicative Corrections

± 1.25

E_f Beam	R Counts / Monitor	ST	RAD	σ_0 10^{-32} cm²/sr BeV	Δ Error in %
2.858	~~0.0013~~ .00104	1.035			
2.828	~~0.00193~~ .00154	1.062			
2.798	~~0.00282~~ .00226	1.081			
2.768	~~0.00202~~ .00162	1.060			
2.738	~~0.00079~~ .00063	0.949		÷ 1.25	
2.708	~~0.00070~~ .00056	0.884	RAD	σ_0 .0118	Δ
2.678	~~0.00072~~ .00058	0.972	~~0.977~~ 0.977	~~0.0148~~	38
2.649	~~0.00129~~ .00103	1.206	1.045	~~0.0356~~ .0285	26
2.620	~~0.00227~~ .00182	0.900	1.158	~~0.0522~~ .0418	17
2.592	~~0.00304~~ .00243	1.013	1.131	~~0.0778~~ .0622	12
2.564	~~0.00291~~ .00233	0.995	1.098	~~0.0717~~ .0574	11
2.536	~~0.00240~~ .00192	0.956	0.961	~~0.0503~~ .0402	12
2.509	~~0.00247~~ .00198	0.951	0.967	~~0.0524~~ .0419	12
2.482	~~0.00264~~ .00211	0.914	0.981	~~0.0571~~ .0457	11
2.455	~~0.00327~~ .00262	0.971	1.040	~~0.0779~~ .0623	10
2.428	~~0.00333~~ .00266	0.964	1.059	~~0.0811~~ .0649	10
2.401	~~0.00523~~ .00418	1.018	1.083	~~0.1390~~ .1112	8
2.375	~~0.00496~~ .00397	1.005	1.063	~~0.1293~~ .1034	8
2.349	~~0.00547~~ .00438	1.010	1.050	0.1429 .1143	8
2.324	~~0.00563~~ .00450	1.007	1.040	~~0.1468~~ .1174	8
2.230	~~0.00603~~ .00482	1.009	1.015	~~0.1554~~ .1243	7
2.274	~~0.00629~~ .00503	1.008	1.009	~~0.1631~~ .1305	7
2.249	~~0.00613~~ .00490	1.000	1.001	~~0.1580~~ .1264	7

* These data are normalized to an elastic scattering cross section 0.8 of Ref 4, because of new measurements of elastic scattering.

Since these data are normalized to the elastic scattering and these are now known to be too high by a factor of two, all cross sections in this table should be lowered by a factor of 2.

Table III (Cont.)

E_f	R	ST	RAD	σ_o	Δ
2.224	~~0.00633~~ .00506	0.998	0.997	~~0.1640~~ .1312	7
2.201	~~0.00767~~ .00614	1.016	1.013	~~0.2075~~ .1660	7
2.177	~~0.00789~~ .00631	1.015	0.997	~~0.2125~~ .1700	6
2.153	~~0.00705~~ .00564	0.998	0.988	~~0.1870~~ .1496	6
2.130	~~0.00801+~~ .00643	1.008	0.979	~~0.2158~~ .1726	5
2.107	~~0.00817~~ .00654	1.006	0.970	~~0.2194~~ .1755	5
2.084	~~0.00760~~ .00608	0.993	0.958	~~0.2009~~ .1607	5
2.061	~~0.00743~~ .00594	0.986	0.936	~~0.1925~~ .1540	4
2.038	~~0.00805~~ .00644	0.993	0.963	~~0.2188~~ .1750	4
2.016	~~0.00865~~ .00692	1.000	0.961	~~0.2389~~ .1911	4
1.994	~~0.00888~~ .00710	1.002	0.956	~~0.2468~~ .1974	4
1.973	~~0.00920~~ .00736	1.006	0.946	~~0.2568~~ .2054	4
1.951	~~0.00883~~ .00706	1.000	0.935	~~0.2450~~ .1960	4
1.930	~~0.00913~~ .00730	1.004	0.933	~~0.2569~~ .2055	4
1.909	~~0.00961~~ .00769	1.010	0.933	~~0.2746~~ .2197	4
1.888	~~0.00941~~ .00753	1.007	0.921	~~0.2677~~ .2142	4
1.868	~~0.00931~~ .00745	1.007	0.904	~~0.2627~~ .2102	4
1.848	~~0.00858~~ .00686	0.995	0.889	~~0.2382~~ .1906	4
1.828	~~0.00888~~ .00710	0.998	0.883	~~0.2481~~ .1985	4
1.808	~~0.00960~~ .00768	1.007	0.884	~~0.2738~~ .2190	4
1.179	~~0.00972~~ .00778	1.008	0.882	~~0.2802~~ .2242	4
1.769	~~0.00941~~ .00752	1.006	0.879	~~0.2743~~ .2194	4
1.750	~~0.00909~~ .00727	1.002	0.877	~~0.2642~~ .2114	4
1.731	~~0.01009~~ .00807	1.014	0.875	~~0.2998~~ .2398	4

Table III (Cont.)

E_f	R	ST	RAD	σ_0	Δ
1.712	~~0.00989~~ .00791	1.014	0.872	~~0.2956~~ .2365	4
1.693	~~0.01005~~ .00804	1.016	0.865	~~0.3020~~ .2416	4
1.676	~~0.00973~~ .00778	1.012	0.860	~~0.2927~~ .2342	4
1.657	~~0.01005~~ .00804	1.016	0.851	~~0.3036~~ .2429	4
1.640	~~0.01048~~ .00838	1.019	0.833	~~0.3142~~ .2514	4
1.622	~~0.01018~~ .00814	1.017	0.848	~~0.3135~~ .2508	5
1.604	~~0.00929~~ .00743	1.007	0.829	~~0.2801~~ .2241	5
1.586	~~0.00868~~ .00694	0.998	0.804	~~0.2545~~ .2036	7
1.569	~~0.00984~~ .00787	1.014	0.776	~~0.2857~~ .2286	7

TABLE IV

Differential Cross Section

$$\frac{d^2\sigma}{d\Omega dE_f} \text{ in } 10^{-32} \text{cm}^2/\text{BeV} - \text{steradian}$$

Averaged over $\Delta K = 150$ MeV centered on $K = 325$ MeV

	31°	90°
$21.4f^{-2}$	no measurement	.855
$25.9f^{-2}$	4.93	no measurement
$35.3f^{-2}$	no measurement	.236
$40.1f^{-2}$	1.24	no measurement

TABLE V

$\sigma_{\perp}$ and $\sigma_{\parallel}$

q^2	$\sigma_{\perp}$	$\sigma_{\parallel}$
25.9	$.98 \pm .25$	$.25 \pm .4$
40.1	$.59 \pm .2$	$.0 \pm .18$

TABLE VI

$\sigma_{long}/\sigma_{trans}$, $N^*(1512)$

prescription	q^2=0.797	1.31	3.30	$(BeV/c)^2$
$\frac{\ell}{\ell+1}$ q^2/K^2	0.797	1.18	2.96	
$\frac{\ell}{\ell+1}$ q^2/q_o^2	0.295	0.312	0.262	
$\frac{\ell}{\ell+1}$ q^2/q_o^{*2}	9.96	601.0	4.12	

TABLE VII

Comparison of Form Factors

q^2 $(BeV/c)^2$	$G_{MV}^2(q^2)/G_{MV}^2(0)$		$G_{EV}(q^2)/G_{EV}(0)$	
0.996	0.0300	0.0319	0.0462	0.0716
1.55	0.00861	0.0114	0.0265	0.0312
3.61	0.000730	0.0012	-0.0059	0.00637
0.791	0.0494	0.0515	0.0689	0.1010
1.31	0.0152	0.0171	0.0254	0.0445
3.30	0.000972	0.00160	-0.0051	0.00760
0.649	0.0750	0.0751	0.0921	0.1370
1.138	0.0217	0.0237	0.00352	0.0570
3.06	0.00126	0.0019	-0.0042	0.00897
0.424	0.154	0.151	0.1516	0.2344
0.822	0.0461	0.0477	0.0648	0.0981
2.69	0.00190	0.0027	-0.0022	0.01156
	1 parameter (Eq. (27))	4 pole (Ref.14)	4 pole	1 parameter

TABLE VIII

Areas under the Resonances, $\frac{\pi}{2} A \Gamma$

(10^{-32} cm^2/sterad)

Resonance	Incident Energy	2.358	2.988	4.874 (BeV)
1.238		0.92	0.31	~~0.0102~~ 0.0082* ÷1.25
1.512		0.98	0.36	~~0.0086~~ .0069* ÷1.25
1.688		0.89	0.33	~~0.0098~~ .0078* ÷1.25
1.920		0.09	0.04	~~0.014~~ .0112* (upper limits ÷1.25.

*~~Since these curves are normalized to elastic scattering, and at this point the elastic scattering is known to be too high by a factor of two, these points should now be divided by 2.~~

~~Some~~ * These data . . .

TABLE IX

"Theoretical" $\sigma_{trans}(q^2, K)$ as extracted from Eq. (35) and (36)

Resonance	Momentum Transfer q^2 =	.996	1.55	3.61	$(BeV/c)^2$
K = .346 BeV M* = 1238 MeV	σ_{tr} =	1.06	0.62	0.052 ~~0.065~~*	$(10^{-28} cm^2)$ ± 1.25

Resonance	Momentum Transfer q^2 =	.797	1.31	3.30
K = .746 BeV M* = 1512 MeV	σ_{tr} =	0.34	0.15	.0046 ~~0.0057~~*

Resonance	Momentum Transfer q^2 =	.649	1.138	3.06
K = 1.045 BeV M* = 1688 MeV	σ_{tr} =	.32	.11	~~.0068~~ .0061 ~~.0076~~*

Resonance	Momentum Transfer q^2 =	.424	.822	2.69
K = 1.50 M* = 1920 MeV	σ_{tr} =	.032	.021	.0016* ~~.020~~

*Since these curves are normalized to elastic scattering and at this point the elastic scattering is known to be too high by a factor of two, these points should now be divided by 2 (25)

TABLE X

1st Order Multipole Dependance of Resonances

		power of q
$N^*(1238)$,	Magnetic Dipole,	$2^1 = 2$
$N^*(1512)$,	Electric Dipole	$2^1 - 2 = 0$
$N^*(1688)$,	Electric Quadrupole	$2^2 - 2 = 2$
$N^*(1920)$,	Magnetic Quadrupole,	$2^4 = 4$

Table A-I

Table of Values of Radiation Kernels Given by Hand, Bjorken and the first approximation

$$K = \frac{\frac{\alpha}{\pi}\left(\ln \frac{q^2}{m^2} - 1\right)}{E - E'}$$

for $q^2 = 1(\text{BeV}/c)^2$, $E = 1\text{BeV}$

	Hand	Bjorken	1st approx.	
$E' = .99E$	3.26	2.9	3.30	
.9	.298	.302	.330	
.8	.135	.144	.165	
.7	.080	.089	.110	$(\text{BeV})^{-1}$
.6	.057	.064	.082	
.5	.042	.048	.066	

Captions to Figures

Fig. 1 A diagram to aid in understanding the kinematics of inelastic ep scattering.

Fig. 2 Layout of the experimental apparatus.

Fig. 3 Arrangement of counters showing a sypical electron trajectory.

Fig. 4 Comparison of the calculated and measured resolution function of the spectrometer.

Fig. 5 A kinematic diagram relating the incident and final electron energies showing the region that must be measured to make a radiative correction.

Fig. 6 Illustration of a process that could produce a false count if care is not taken.

Fig. 7 Spectrum of inelastically scattered electrons for $\theta=31^{\circ}$ and $E_1=2.358$ BeV (data of Table II). The dashed line shows the radiative correction applied.

Fig. 8 As for Fig. 7, $\theta=31^{\circ}$, $E_1=2.988$ BeV data of Table II.

Fig. 21 The resonant N^*=1512 MeV cross section plotted against $(q/K)^2$ showing the unusually high electroproduction cross section.

Fig. 22 The resonant N^*=1688 MeV cross section showing a fit to electric quadrupole excitation.

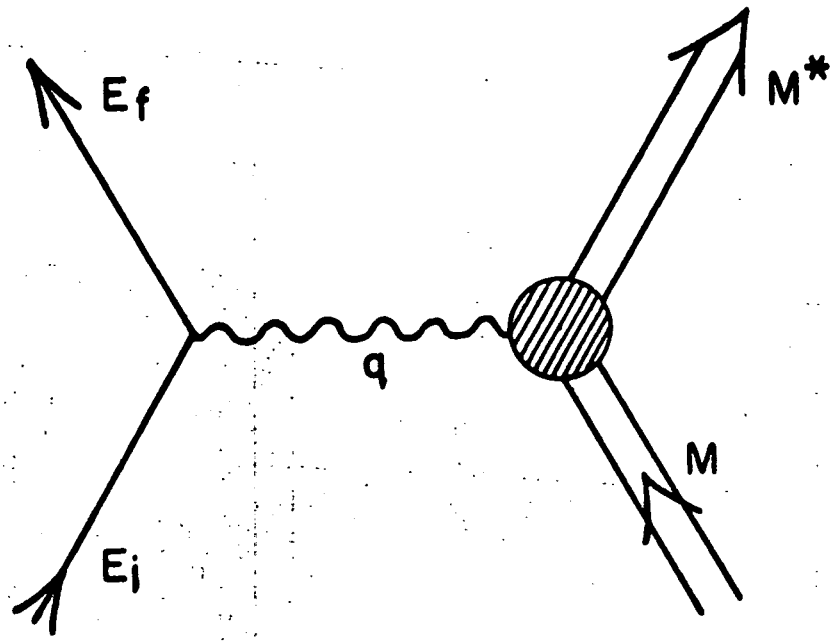
E_f
M^*
q
M
E_i

1

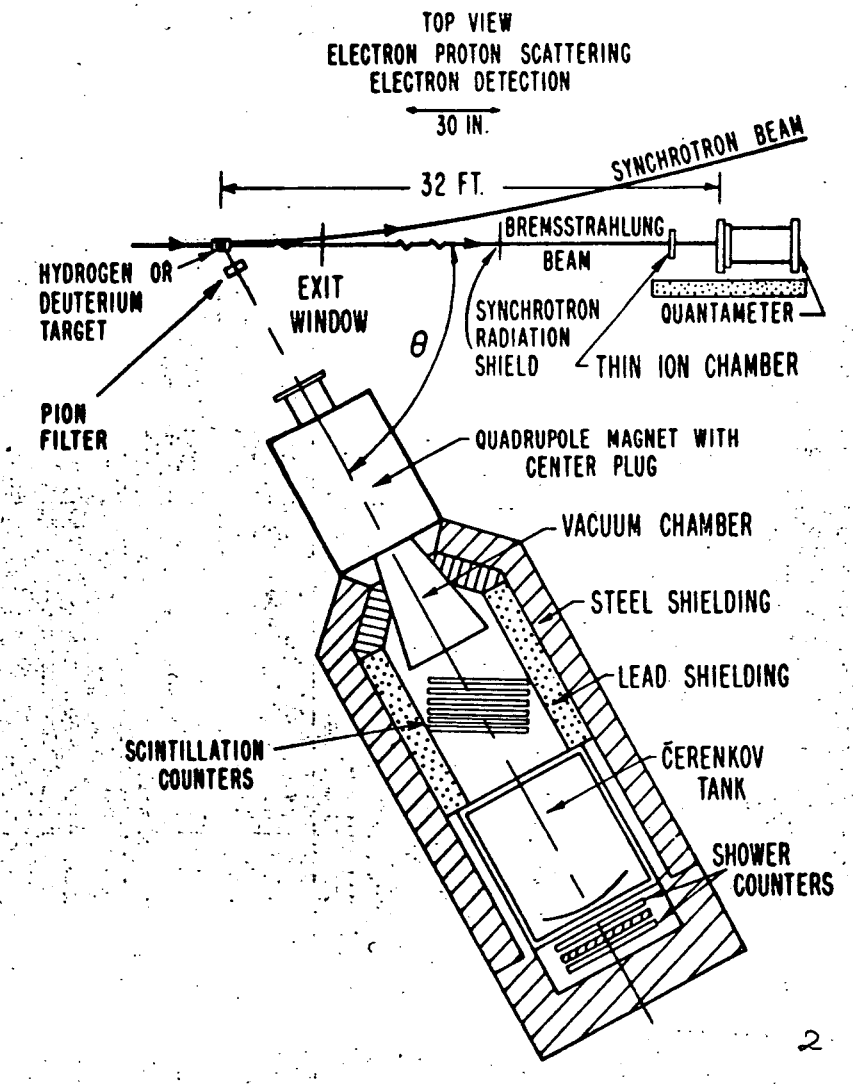
TOP VIEW
ELECTRON PROTON SCATTERING
ELECTRON DETECTION
30 IN.
32 FT.
SYNCHROTRON BEAM
BREMSSTRAHLUNG BEAM
HYDROGEN OR DEUTERIUM TARGET
EXIT WINDOW
θ
SYNCHROTRON RADIATION SHIELD
QUANTAMETER
THIN ION CHAMBER
PION FILTER
QUADRUPOLE MAGNET WITH CENTER PLUG
VACUUM CHAMBER
STEEL SHIELDING
LEAD SHIELDING
SCINTILLATION COUNTERS
ČERENKOV TANK
SHOWER COUNTERS

2

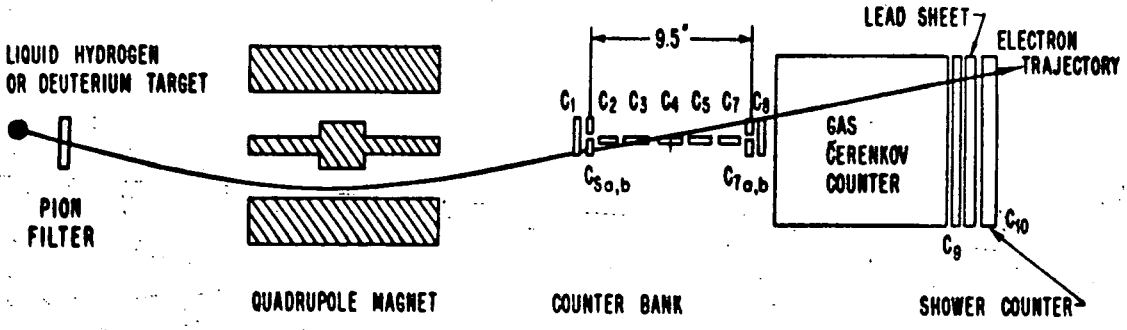

ELECTRON DETECTION APPARATUS

3

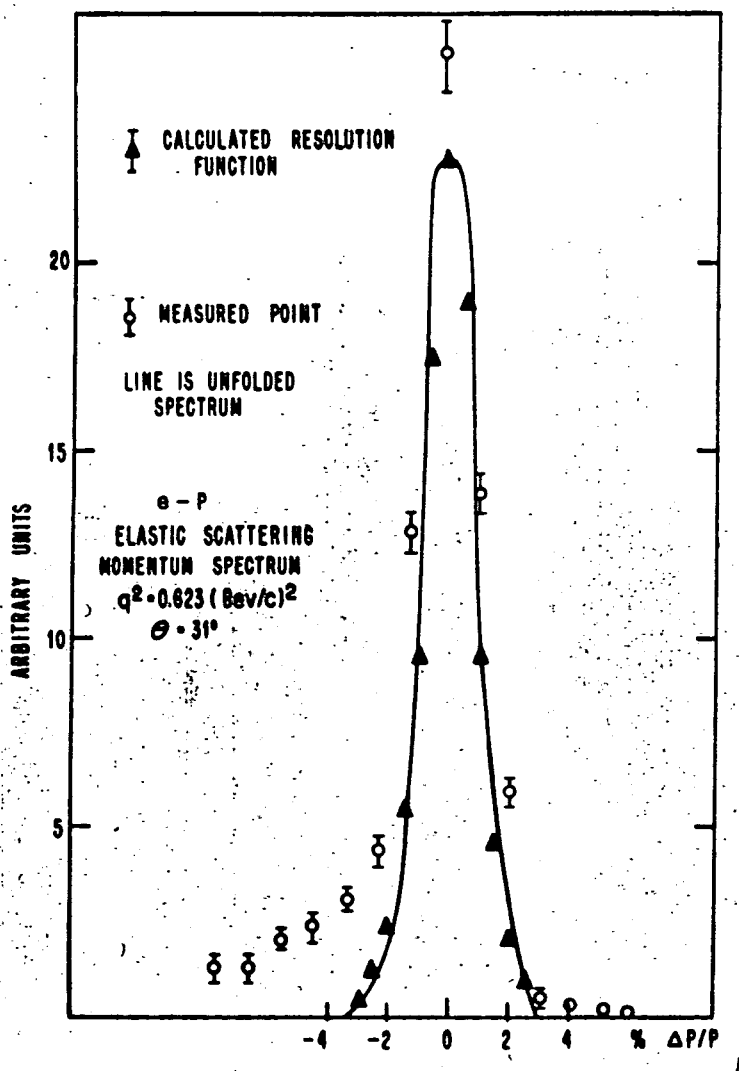

4

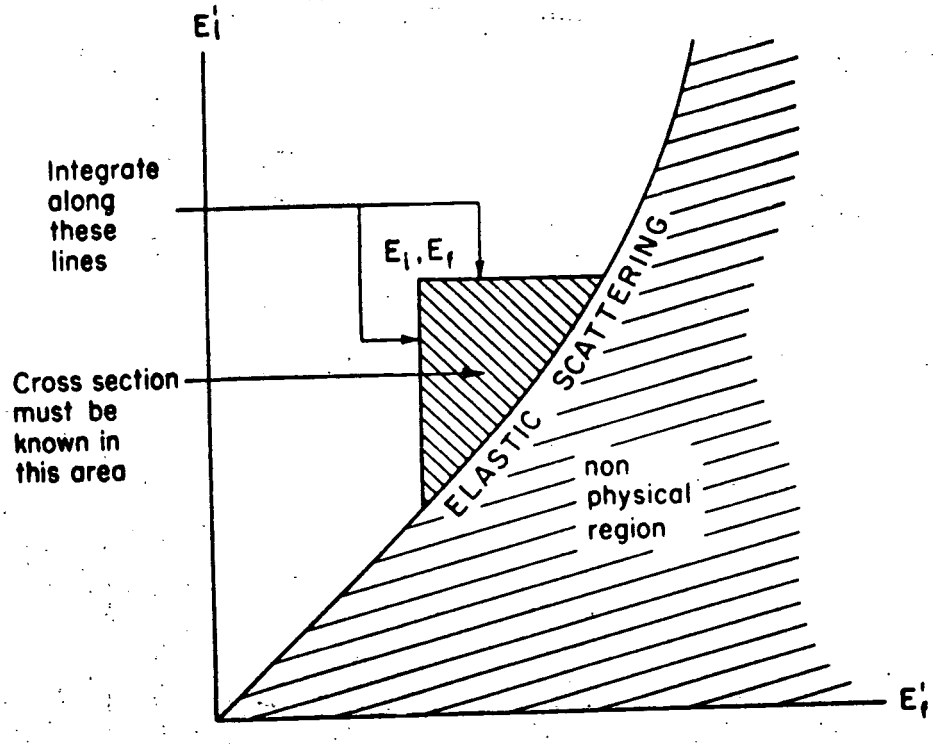

5

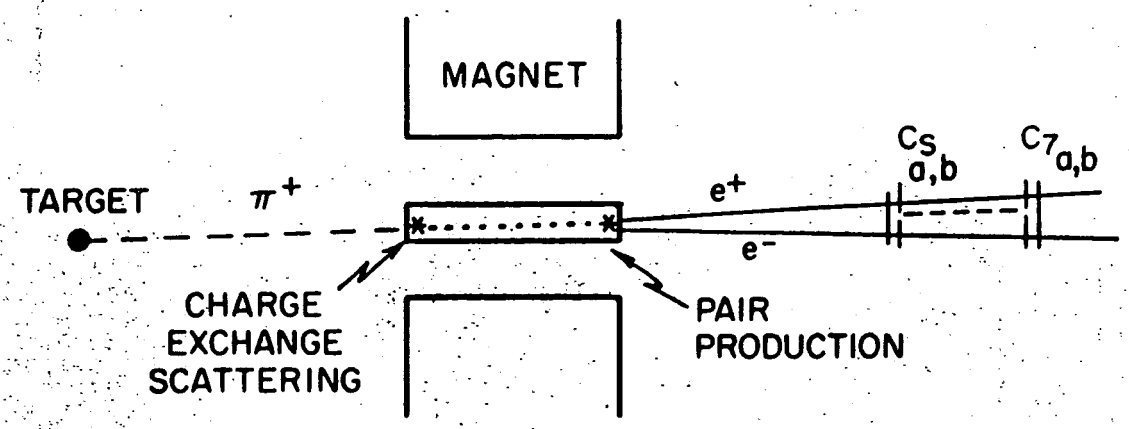

ILLUSTRATION OF A PROCESS THAT CAN PRODUCE A FALSE KINEMATIC COINCIDENCE COUNT.

6

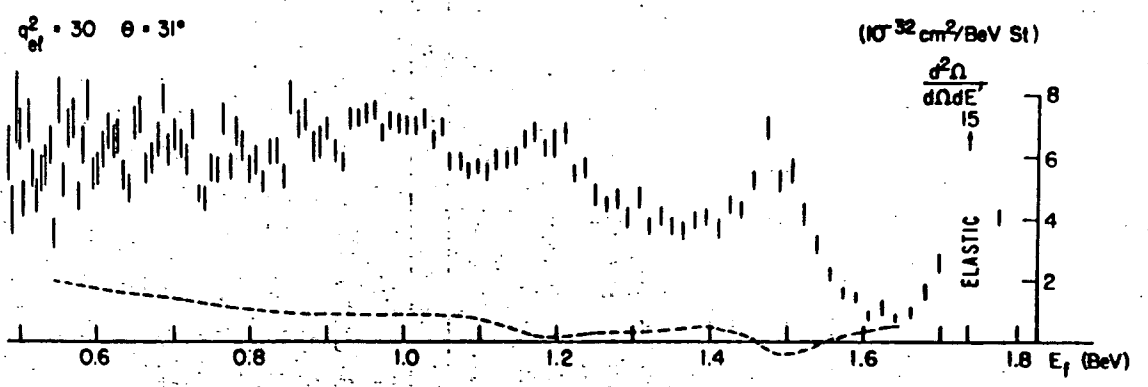
q^2_{el} = 30 θ = 31°
$(10^{-32}\ cm^2/BeV\ St)$
$\frac{d^2\Omega}{d\Omega dE'}$
15
ELASTIC
8
6
4
2
0.6
0.8
1.0
1.2
1.4
1.6
1.8
E_f (BeV)

7

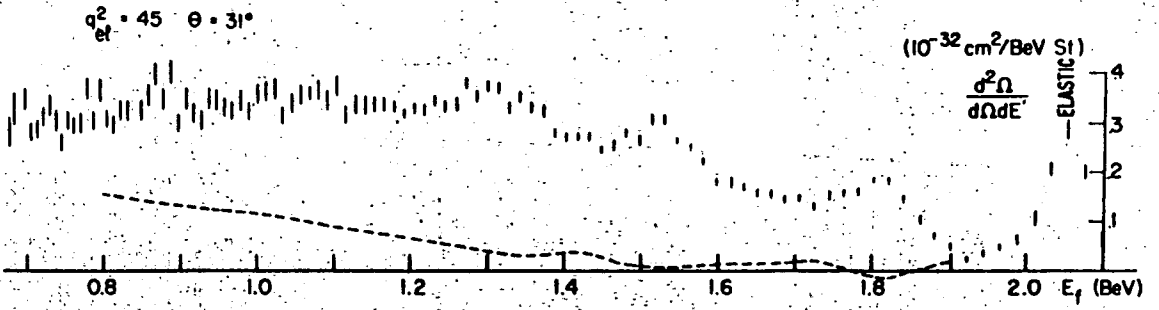
q^2_{el} = 45 θ = 31°
$(10^{-32}\ cm^2/BeV\ St)$
$\frac{d^2\Omega}{d\Omega dE'}$
ELASTIC
4
3
2
1
0.8
1.0
1.2
1.4
1.6
1.8
2.0
E_f (BeV)

8

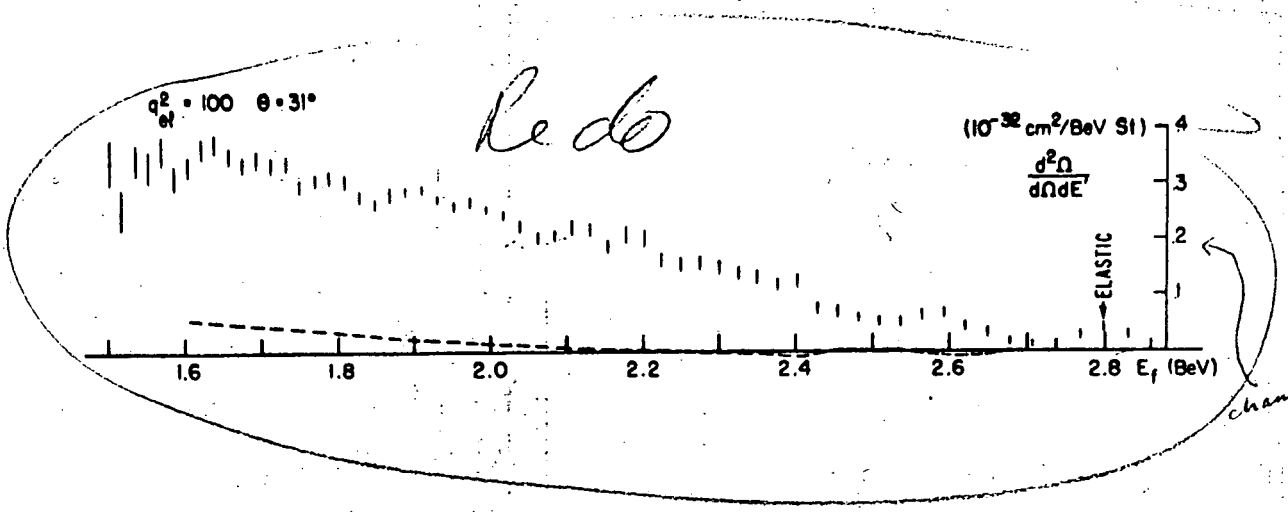
q^2_{el} = 100 θ = 31°
Redo
$(10^{-32}$ cm^2/BeV St)
$\frac{d^2\Omega}{d\Omega dE'}$
ELASTIC
1.6
1.8
2.0
2.2
2.4
2.6
2.8 E_f (BeV)
change scale.

9

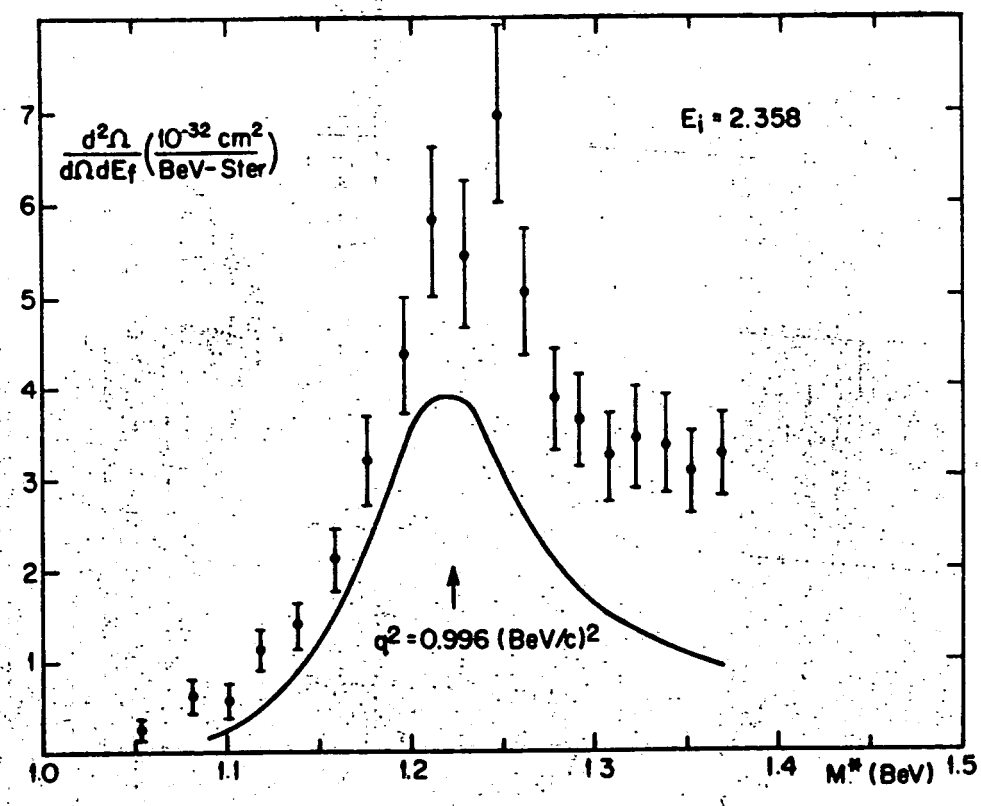
$\frac{d^2\Omega}{d\Omega dE_f}\left(\frac{10^{-32}\text{ cm}^2}{\text{BeV-Ster}}\right)$
E_i = 2.358
q^2 = 0.996 (BeV/c)^2
1.0
1.1
1.2
1.3
1.4
1.5
M^* (BeV)

10

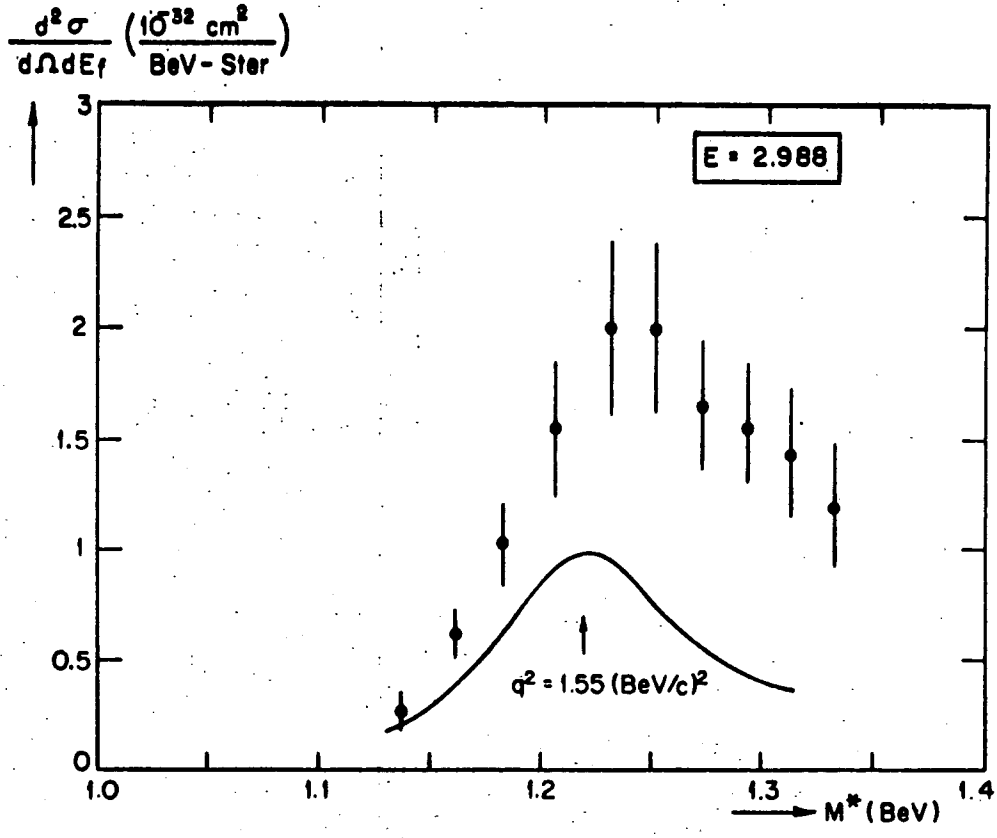
$\frac{d^2\sigma}{d\Omega dE_f}\left(\frac{10^{32}\ cm^2}{BeV\text{-}Ster}\right)$
E = 2.988
q^2 = 1.55 (BeV/c)^2
M* (BeV)
0
0.5
1
1.5
2
2.5
3
1.0
1.1
1.2
1.3
1.4

11

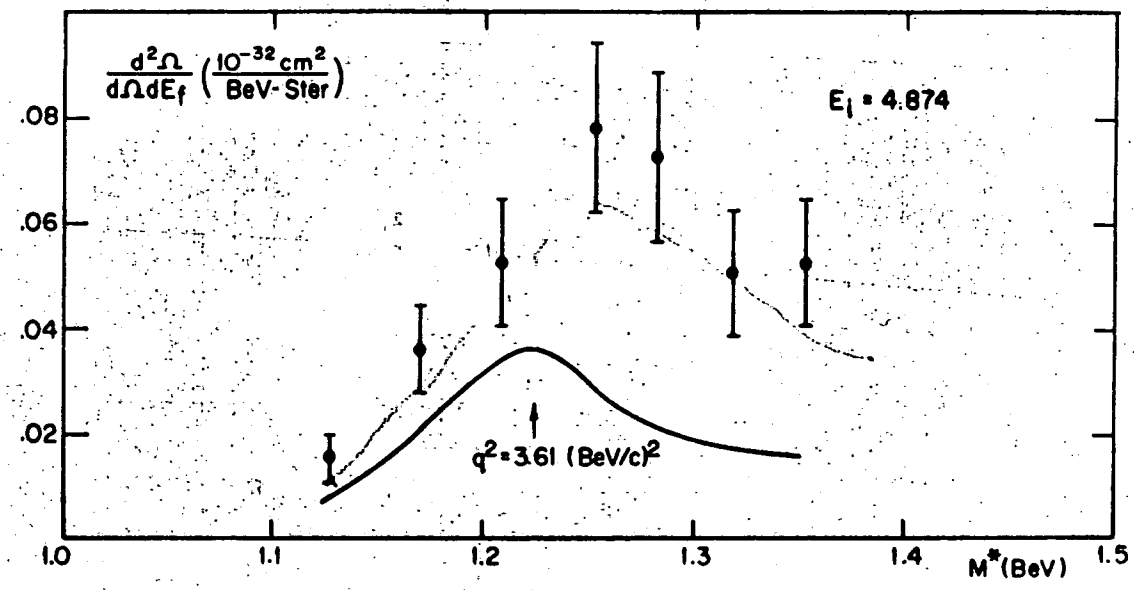
$\frac{d^2\Omega}{d\Omega dE_f}\left(\frac{10^{-32}\ cm^2}{BeV\text{-}Ster}\right)$
E_l = 4.874
q^2 = 3.61 (BeV/c)^2
M*(BeV)
.02
.04
.06
.08
1.0
1.1
1.2
1.3
1.4
1.5

12

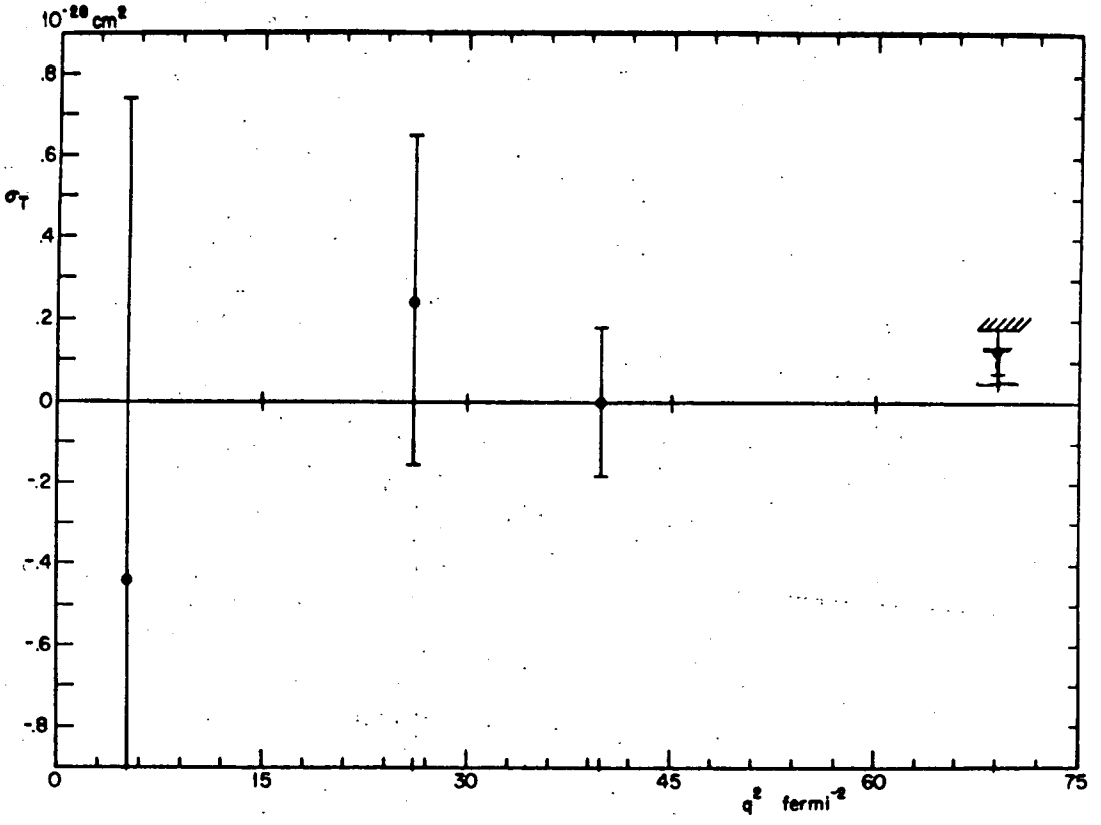
10^{-28} cm^2
σ_T
.8
.6
.4
.2
0
-.2
-.4
-.6
-.8
0
15
30
45
60
75
q^2 fermi^{-2}

13

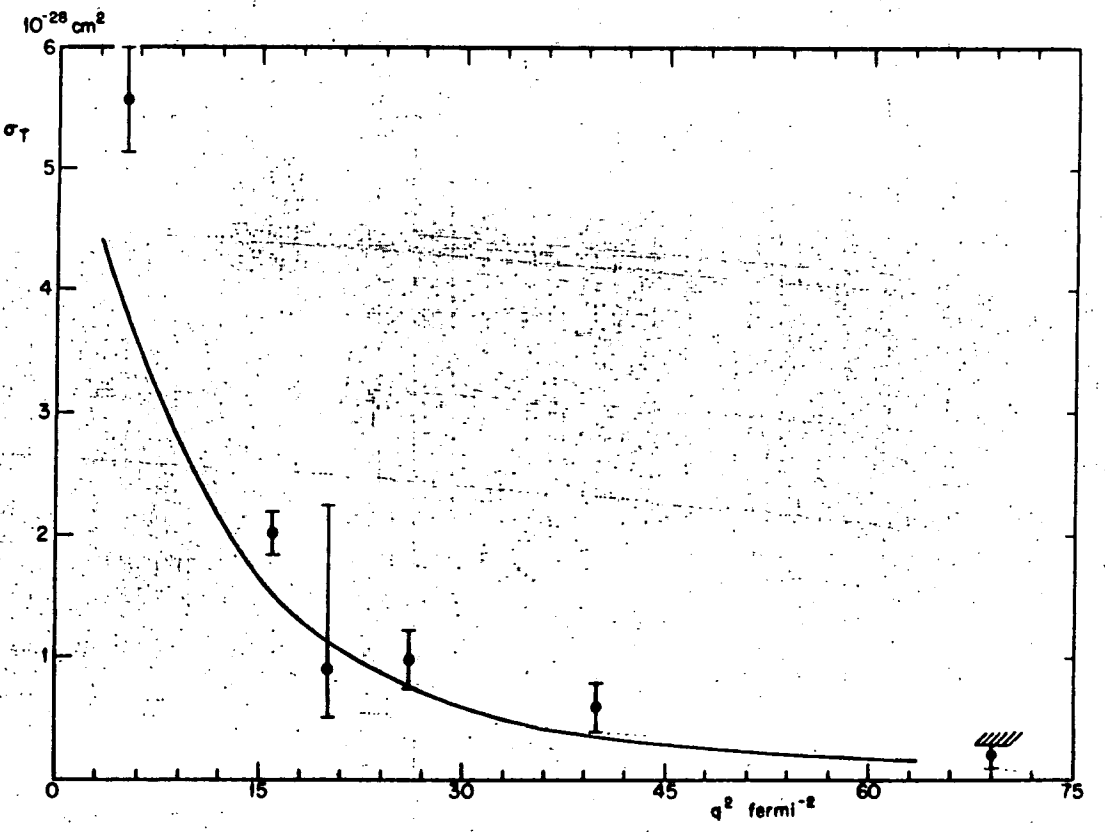
10^{-28} cm^2
σ_T
6
5
4
3
2
1
0
15
30
45
60
75
q^2 fermi^{-2}

14

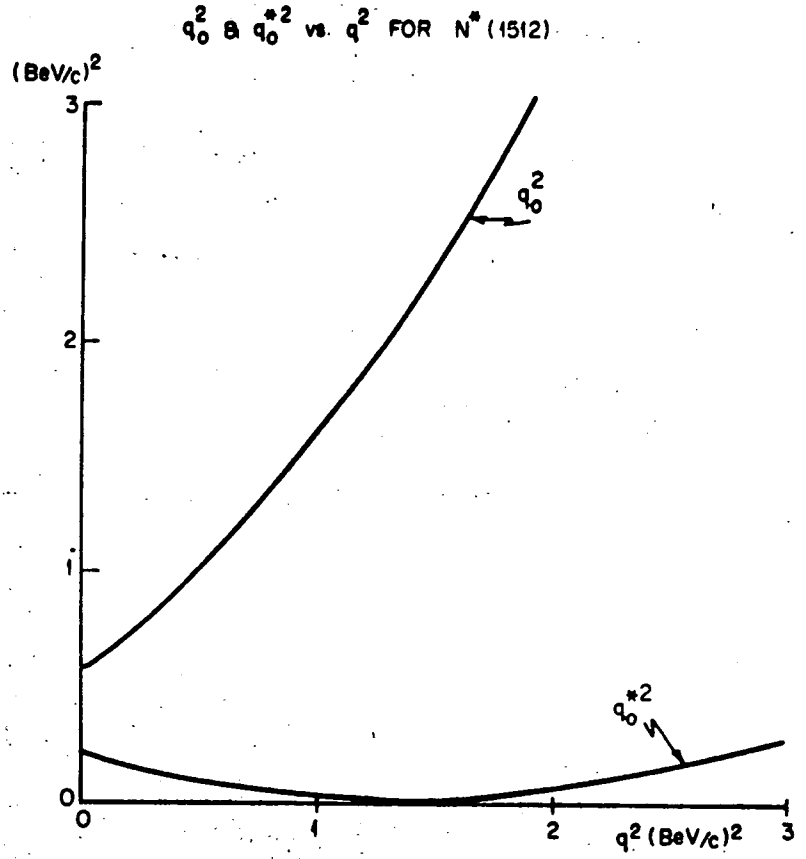
q_0^2 & q_0^{*2} vs. q^2 FOR $N^*(1512)$
$(BeV/c)^2$
3
2
1
0
q_0^2
q_0^{*2}
0
1
2
3
$q^2\ (BeV/c)^2$

15

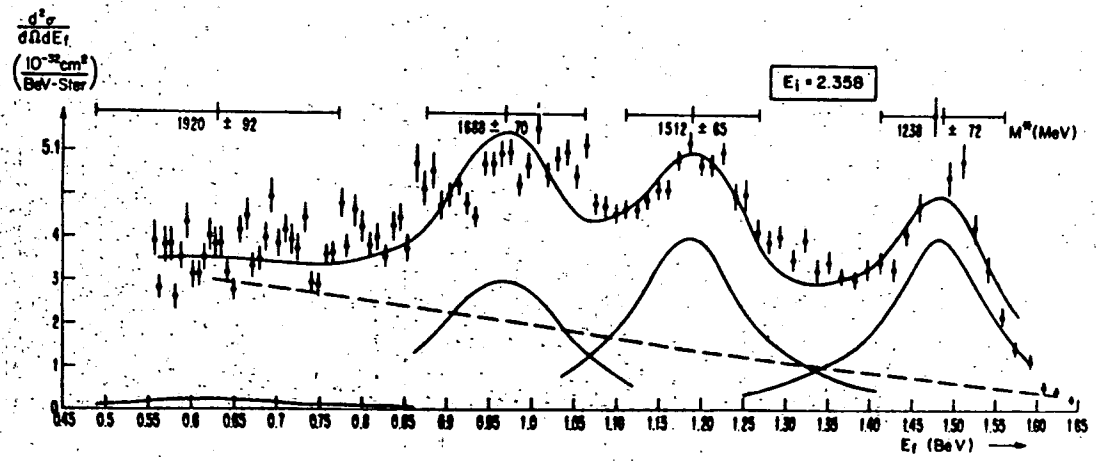
$\frac{d^2\sigma}{d\Omega dE_f}$
$\left(\frac{10^{-32}cm^2}{BeV\text{-}Ster}\right)$
$E_i = 2.358$
1920 ± 92
1688 ± 70
1512 ± 65
1238 ± 72
$M^*(MeV)$
5.1
4
3
2
1
0
0.45 0.5 0.55 0.6 0.65 0.7 0.75 0.8 0.85 0.9 0.95 1.0 1.05 1.10 1.15 1.20 1.25 1.30 1.35 1.40 1.45 1.50 1.55 1.60 1.65
E_f (BeV) ⟶

16

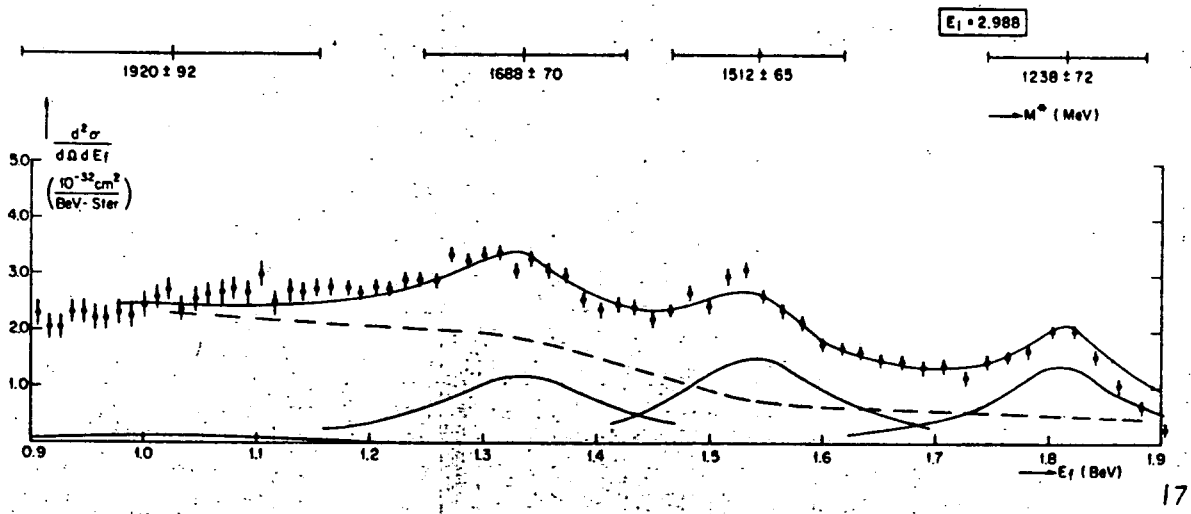
E_I = 2.988
1920 ± 92
1688 ± 70
1512 ± 65
1238 ± 72
M* (MeV)
$\frac{d^2\sigma}{d\Omega\, dE_f}$
$\left(\frac{10^{-32}cm^2}{BeV\text{-}Ster}\right)$
5.0
4.0
3.0
2.0
1.0
0.9
1.0
1.1
1.2
1.3
1.4
1.5
1.6
1.7
1.8
1.9
E_f (BeV)

17

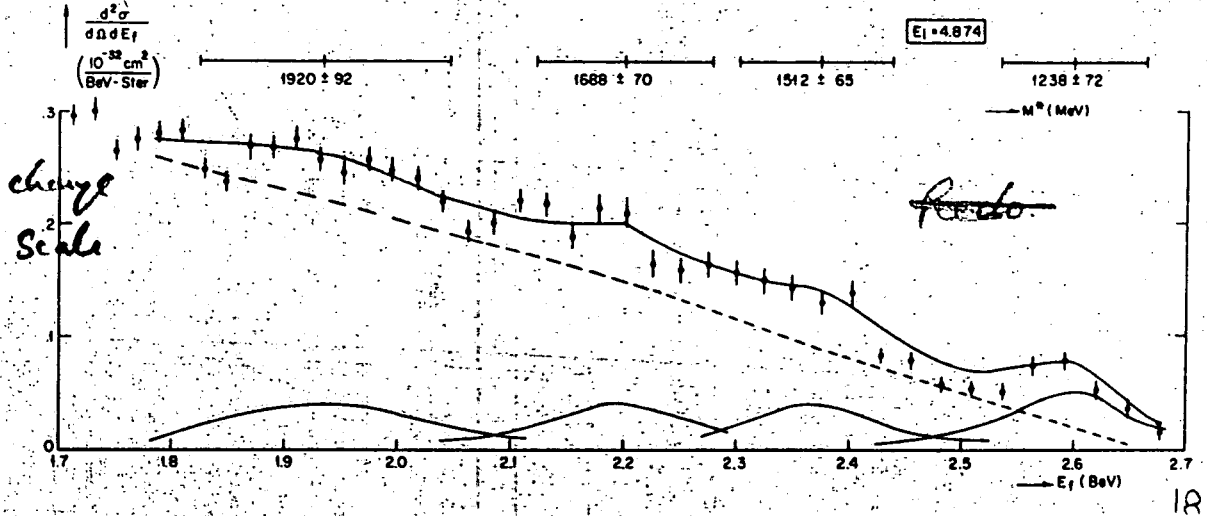
$\frac{d^2\sigma}{d\Omega\, dE_f}$
$\left(\frac{10^{-32}cm^2}{BeV\text{-}Ster}\right)$
E_I = 4.874
1920 ± 92
1688 ± 70
1512 ± 65
1238 ± 72
M* (MeV)
change
Scale
3
2
1
0
1.7
1.8
1.9
2.0
2.1
2.2
2.3
2.4
2.5
2.6
2.7
E_f (BeV)

18

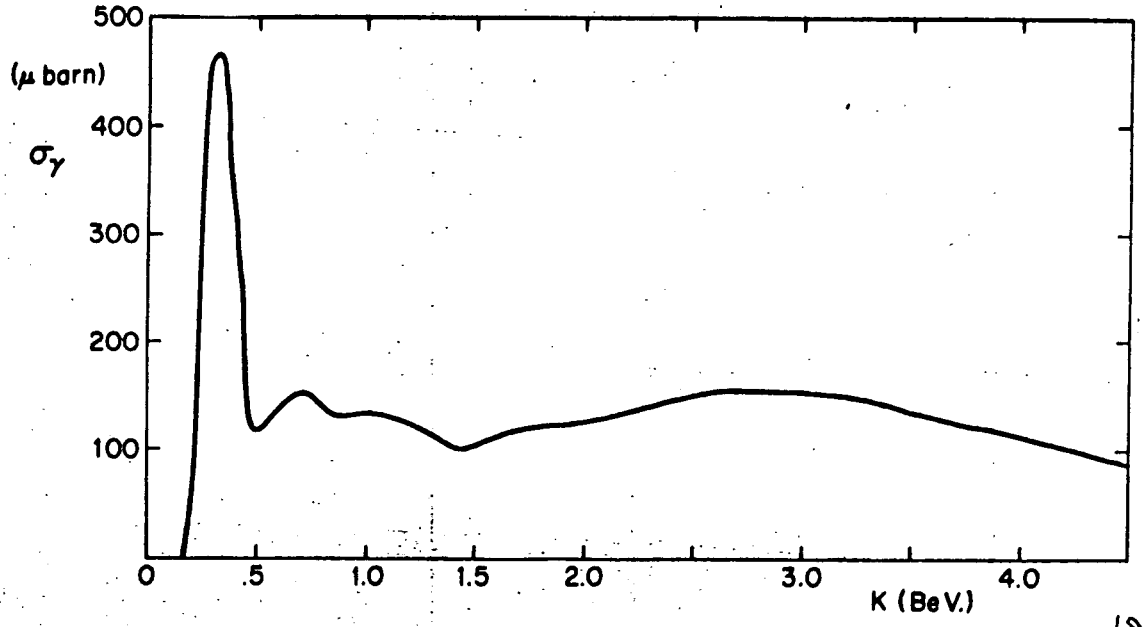
500
(μ barn)
σ_γ
400
300
200
100
0
.5
1.0
1.5
2.0
3.0
4.0
K (BeV.)

19

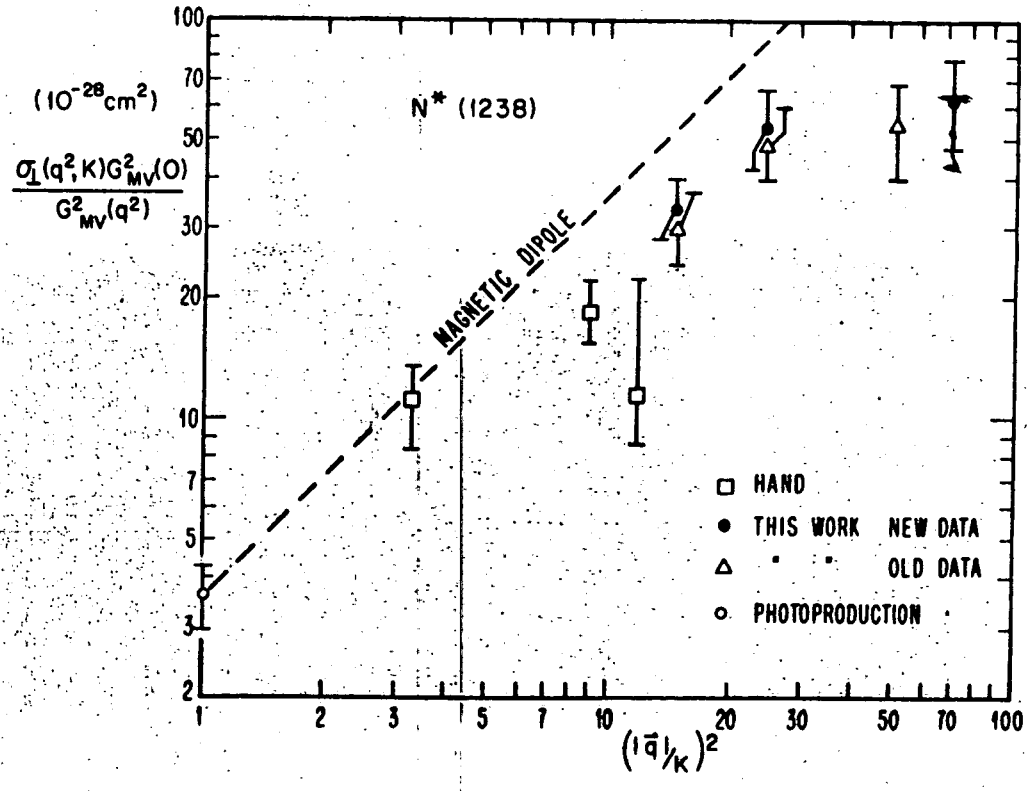
100
70
50
30
20
10
7
5
3
2
$(10^{-28}cm^2)$
$\frac{\sigma_\perp(q^2,K)G^2_{MV}(0)}{G^2_{MV}(q^2)}$
N* (1238)
MAGNETIC DIPOLE
HAND
THIS WORK NEW DATA
OLD DATA
PHOTOPRODUCTION
1
2
3
5
7
10
20
30
50
70
100
$(|\vec{q}|/K)^2$

20

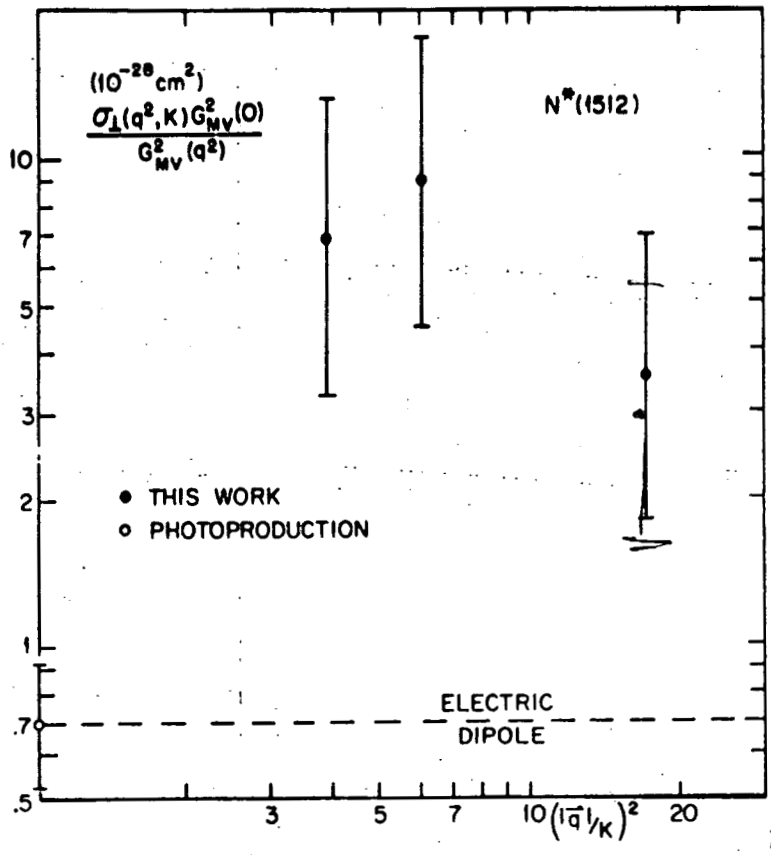
$(10^{-28}cm^2)$
$\frac{\sigma_\perp(q^2,K)G^2_{MV}(0)}{G^2_{MV}(q^2)}$
N*(1512)
10
7
5
3
2
1
.7
.5
● THIS WORK
○ PHOTOPRODUCTION
ELECTRIC DIPOLE
3
5
7
10
$(|\vec{q}|/K)^2$
20

21

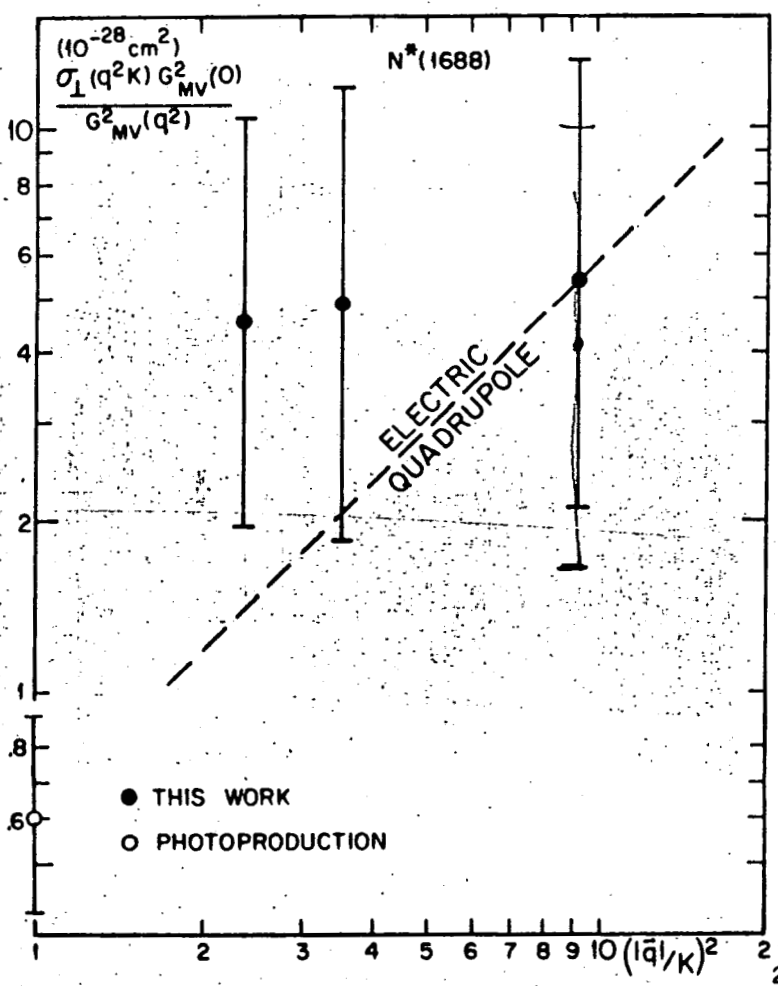
$(10^{-28}cm^2)$
$\frac{\sigma_\perp(q^2K)\,G^2_{MV}(0)}{G^2_{MV}(q^2)}$
N*(1688)
10
8
6
4
2
1
.8
.6
ELECTRIC QUADRUPOLE
● THIS WORK
○ PHOTOPRODUCTION
1
2
3
4
5
6
7
8
9
10
$(|\vec{q}|/K)^2$
2

22